European Journal of Applied Mathematics (2026), **37**, pp. 1313–1341
doi:10.1017/S0956792526100357

CAMBRIDGE UNIVERSITY PRESS

PAPERS

Global bifurcations and pattern formation in target–offender–guardian crime models

Madi Yerlanov[1], Qi Wang[2] and Nancy Rodríguez[1]

[1]Applied Mathematics, University of Colorado Boulder, Boulder, USA
[2]Mathematics, Howard University, Washington, USA
Corresponding author: Madi Yerlanov; Email: madi.yerlanov@colorado.edu

Received: 17 September 2025; **Revised:** 19 February 2026; **Accepted:** 19 February 2026;
First published online: 23 March 2026

Keywords: Urban crime model; steady-state bifurcation; Hopf bifurcation; pattern formation; chaos

2020 Mathematics Subject Classification: 35B36 (Primary); 70K50, 91D99 (Secondary)

Abstract

We study a reaction–advection–diffusion model of a target–offender–guardian system designed to capture interactions between urban crime and policing. Using Crandall–Rabinowitz bifurcation theory and spectral analysis, we establish rigorous conditions for both steady-state and Hopf bifurcations. These results identify critical thresholds of policing intensity at which spatially uniform equilibria lose stability, leading either to persistent heterogeneous hotspots or oscillatory crime–policing cycles. From a criminological perspective, such thresholds represent tipping points in guardian mobility: once crossed, they can lock neighbourhoods into stable clusters of criminal activity or trigger recurrent waves of hotspot formation. Numerical simulations complement the theory, exhibiting stationary patterns, periodic oscillations and chaotic dynamics. By explicitly incorporating law enforcement as a third interacting component, our framework extends classical two-equation models. It offers new tools for analysing non-linear interactions, bifurcations and pattern formation in multi-agent social systems.

1. Introduction

We study an initial-boundary value problem for (A, ρ, u), defined on the space-time domain $(\mathbf{x}, t) \in \Omega \times (0, T]$, where $\Omega \subset \mathbb{R}^N$ is a bounded domain with piecewise smooth boundary $\partial\Omega$, and the time horizon $T > 0$

$$\begin{cases} \dfrac{\partial A}{\partial t} = D_A \Delta A - A + \alpha + A\rho, & \text{in } \Omega \times (0, T], \\ \dfrac{\partial \rho}{\partial t} = \nabla \cdot \left(D_\rho \nabla \rho - 2\rho \nabla \ln A \right) - A\rho + \beta - \rho u, & \text{in } \Omega \times (0, T], \\ \dfrac{\partial u}{\partial t} = \nabla \cdot \left(D_u \nabla u - \chi u \nabla \ln A \right), & \text{in } \Omega \times (0, T], \\ \dfrac{\partial A}{\partial \mathbf{n}} = \dfrac{\partial \rho}{\partial \mathbf{n}} = \dfrac{\partial u}{\partial \mathbf{n}} = 0, & \text{on } \partial\Omega, \\ (A, \rho, u)(\mathbf{x}, 0) = (A_0, \rho_0, u_0) \geq, \not\equiv 0, & \text{in } \Omega. \end{cases} \tag{E}$$

Here, ∂ denotes partial differentiation with respect to time t, while ∇ and Δ represent the spatial gradient and Laplacian operators, respectively. The parameters D_A, D_ρ, D_u, α, and β are assumed to be positive constants, whereas χ may take either positive or negative values, depending on the modelling context, as

© The Author(s), 2026. Published by Cambridge University Press. This is an Open Access article, distributed under the terms of the Creative Commons Attribution licence (https://creativecommons.org/licenses/by/4.0/), which permits unrestricted re-use, distribution and reproduction, provided the original article is properly cited.

https://doi.org/10.1017/S0956792526100357 Published online by Cambridge University Press

discussed later. The zero-flux (Neumann) boundary conditions, expressed via $\frac{\partial}{\partial \mathbf{n}}$, are imposed to model an enclosed environment. The initial conditions are assumed to be nonnegative and not identically zero; this, together with the strong maximum principle, ensures that each component (A, ρ, u) remains strictly positive for all $t > 0$. Finally, the terminal time T represents the time horizon for the analysis: it is taken as infinite in theoretical investigations and sufficiently large in numerical simulations to capture the system's long-term behaviour.

1.1. The UCLA model

System (E) can be used to model the spatio-temporal evolution of urban criminal activity under the influence of police patrol intervention. Specifically, it describes the dynamics of the population density ρ of criminal agents, who are attracted to regions with high attractiveness A and are deterred by the presence of law enforcement, represented by u. This approach to modelling urban crime traces back to the seminal work [48] of a UCLA team in 2008, which was inspired by theories such as routine activity theory, the broken-windows effect and the repeat and near-repeat victimization effect [43, 60]. They developed a two-dimensional agent-based lattice model that captures both the movement of offenders and the evolution of local attractiveness. In the spatial continuum limit, this discrete model leads to a fully coupled system of partial differential equations:

$$\begin{cases} \dfrac{\partial A}{\partial t} = D_A \Delta A - A + A_0 + A\rho, & \text{in } \Omega \times (0, T], \\ \dfrac{\partial \rho}{\partial t} = \nabla \cdot (D_\rho \nabla \rho - 2\rho \nabla \ln A) - A\rho + \bar{B}, & \text{in } \Omega \times (0, T]. \end{cases} \tag{1.1.1}$$

The linear diffusion coefficient D_A represents the effect of the near-repeat victimization phenomenon. Since the expected number of crimes is given by the product $A\rho$, the self-exciting nature of crime is incorporated into the dynamics through the $+A\rho$ term in the first equation. When a crime occurs, it is assumed that the perpetrator is removed, leading to the $-A\rho$ term in the second equation. External sources of growth, which may vary in space and time, are also considered for both variables and are denoted by A_0 and $\bar{B}$, respectively. Finally, we note that the movement of offenders combines random motion, modelled by linear diffusion, with a directional bias towards regions of high attractiveness – resulting in a chemotaxis-like drift. We refer interested readers to [19, 48] for detailed derivations and further justification of system (1.1.1) and to [12, 18] for reviews of agent-based models in urban crime modelling.

The UCLA continuum model and its 2D lattice counterpart have gained significant academic recognition for their ability to simulate complex spatio-temporal dynamics and generate both regular and irregular spatial patterns. Most notably, these models successfully capture the aggregation phenomena, commonly known as hotspots, in urban criminal activity, providing critical insights into the spatial distribution of crime. The global well-posedness of the model in (1.1.1) is investigated in [14, 21, 38, 40, 55, 61]. These studies have established that the system admits a unique global-in-time solution, which remains uniformly bounded in one-dimensional settings or in higher dimensions when the advection effect is weak or sublinear. More importantly, a substantial body of research, including [4, 8, 17, 19, 20, 24, 28, 29, 30, 32, 46, 47, 53], has focused on the emergence of nontrivial spatial patterns. These works demonstrate that system (1.1.1) can produce structured crime hotspots, represented by spatially concentrated profiles that may be either stationary or time-dependent, thereby successfully capturing the characteristic features of urban residential burglary. Building on these foundations, researchers have extended the theoretical framework of system (1.1.1) to model real-world crime dynamics more accurately. They include the study of non-linear or anomalous diffusion and spatial heterogeneity in both the near-repeat victimization effect and the dispersal strategies of offenders [19, 31]; modelling criminal movement using Lévy processes [9, 27, 35]; incorporating age-structured populations [25, 42] and examining geographic profiling [33]. For reviews in this area, we refer the reader to [3, 4, 12, 34].

https://doi.org/10.1017/S0956792526100357 Published online by Cambridge University Press

1.2. The UCLA model with policing force

Given that crime and disorder are unevenly distributed across urban areas, scholars and practitioners in [13, 15, 44, 49, 57, 58] have advocated for concentrating policing efforts in high-demand zones rather than dispersing resources uniformly across the city. This strategy, commonly referred to as "hot-spot policing" or "hotspotting, " emphasizes geographic precision, focusing on the location of crimes rather than the characteristics of individual offenders. While this targeted approach has demonstrated measurable short-term reductions in crime, its broader effectiveness remains the subject of debate. Critics (*cf.*, [5, 6, 15, 23, 41, 59]) have raised concerns about potential unintended consequences, such as the spatial displacement of crime, the erosion of community trust and the risk of over-policing marginalized neighbourhoods. Moreover, questions remain about how different policing strategies interact with the underlying social and economic dynamics that drive criminal behaviour. These challenges highlight the need for more comprehensive models that not only track where crime occurs but also capture how policing interventions influence the evolving spatial patterns of crime over time.

A major extension of the original model proposed by the UCLA team involves incorporating the effects of policing strategies on the evolution of criminal activity. In particular, the authors of [22, 36] independently introduced an additional equation to represent police deployment and targeted patrols. These papers adopt different modelling frameworks and assign distinct roles to law enforcement. In this work, we follow the formulation introduced in the later study [54], which in turn builds on the continuum model of [37], itself a generalization of the earlier approach in [36]:

$$u_t = \nabla \cdot (D_u \nabla u - \chi u \nabla \ln A),$$

where u denotes the distribution of law enforcement in the field. The positive parameters D_u and χ represent the intensity of the random movement of police and their response to criminal activity, respectively. Incorporating an explicit law enforcement component allows one to systematically study how various patrol strategies, whether reactive or proactive, affect hotspot formation, stability and suppression under different assumptions about agent movement and crime-attractiveness feedback. When $\chi > 0$, law enforcement agents tend to migrate towards areas with high attractiveness, whereas $\chi < 0$ corresponds to a strategy in which police are deployed to regions of low attractiveness.

From a modelling perspective, one may question the realism of choosing $\chi < 0$. In particular, it remains unclear whether deploying police resources to low-crime areas yields clear benefits [2]. Nevertheless, we allow $\chi < 0$ in our formulation to avoid imposing additional constraints solely to guarantee positivity. We also identify a second important threshold at $\chi = 2$, corresponding to the regime in which police movement matches that of crime agents. The two values $\chi = 0$ and $\chi = 2$ will therefore play a central role in the numerical simulations presented in this paper. In addition, we identify other critical χ-thresholds associated with the onset of various bifurcations. Together, these critical parameter values determine the qualitative behaviour of the system. Consequently, changes in police response intensity may fundamentally reshape the spatial crime landscape. The sign and magnitude of χ thus encode different policing strategies and can be chosen according to the specific modelling objectives.

While adding a third equation to model law enforcement enhances the system's realism by incorporating police deployment strategies, it also introduces new mathematical challenges, particularly in analysing pattern formation and stability. The resulting three-component reaction–diffusion system (E) has been examined by several researchers to explore how policing influences crime dynamics. Tse and Ward [54] conducted a detailed singular perturbation analysis of (E) in one dimension, constructing steady-state hotspot (spike) solutions and performing a nonlocal eigenvalue analysis to characterize their linear stability. They distinguished between synchronous and asynchronous instabilities, showing that hotspot locations may destabilize either in phase (oscillating together) or out of phase (oscillating asynchronously), depending on police response and other system parameters. These results highlight how law enforcement strategies shape the temporal dynamics of urban crime distributions. Building on this foundation, Buttenschoen et al. [7] refined the linear stability framework and focused more explicitly on how targeted policing strategies influence hotspot selection and stabilization. Their work strengthens the

https://doi.org/10.1017/S0956792526100357 Published online by Cambridge University Press

connection between the number and spacing of spikes and the intensity of police deployment, demonstrating, for example, that increasing the strength or spatial focus of policing can shift the threshold for hotspot instability.

Rodríguez et al. [39] applied bifurcation theory to rigorously establish the existence of stable spatial and temporal patterns (steady states and periodic orbits), identify critical thresholds for pattern emergence and analyse wavemode selection. Strikingly, they showed that anti-hotspot policing – dispatching police away from areas of high attractiveness – can stabilize crime hotspots and suppress oscillations. Although they proved global existence and boundedness of solutions, their analysis also revealed that the system may exhibit ill-posedness due to strong sensitivity to initial conditions, raising concerns about its predictive reliability. Further studies of system (E) can be found in [16, 37, 62, 63], where the extended model has been examined under different contexts. Collectively, these works demonstrate that the system supports a broad spectrum of dynamic behaviours – including spatially uniform equilibria, spatially heterogeneous steady states, periodic oscillations and even chaotic patterns. Numerical simulations across the literature not only validate the theoretical predictions but also underscore the model's inherent richness and complexity.

1.3. Preliminaries and outline

Before detailing our main steps and contributions, we first note that in this framework, homogeneous Neumann boundary conditions imply a fixed number of guardians throughout all temporal dynamics as

$$\frac{d}{dt}\int_{\Omega} u(\mathbf{x},t)d\mathbf{x} = 0 \quad \forall t > 0.$$

If we introduce a parameter λ to represent the spatial average of A, then the system admits the following positive constant steady state

$$\bar{A} := \lambda,\ \ \bar{\rho} := 1 - \frac{\alpha}{\lambda},\ \ \bar{u} := \frac{1}{|\Omega|}\int_{\Omega} u_0(\mathbf{x})\, d\mathbf{x} = \lambda\left(\frac{\beta}{\lambda-\alpha} - 1\right), \tag{SS}$$

each of which is positive under the condition

$$\alpha < \lambda < \alpha + \beta.$$

Our study focuses on spatially heterogeneous solutions of system (E) that extend beyond the homogeneous patterns described by (SS). To characterize the system's long-term behaviour, we analyse its steady states, natural candidates for dynamical attractors, by seeking nonconstant positive solutions to the following coupled system:

$$\begin{cases} 0 = D_A\Delta A - A + \alpha + A\rho, & \text{in } \Omega, \\ 0 = \nabla\cdot(D_\rho\nabla\rho - 2\rho\nabla\ln A) - A\rho + \beta - \rho u, & \text{in } \Omega, \\ 0 = \nabla\cdot(D_u\nabla u - \chi u\nabla\ln A), & \text{in } \Omega, \\ \dfrac{\partial A}{\partial \mathbf{n}} = \dfrac{\partial \rho}{\partial \mathbf{n}} = \dfrac{\partial u}{\partial \mathbf{n}} = 0, & \text{on } \partial\Omega. \end{cases} \tag{EQ}$$

The interaction between spatial heterogeneity and non-linear coupling creates significant mathematical challenges, and a deeper analysis is needed to fully understand the resulting dynamics. While prior studies in [7, 16, 39, 54, 63] have shown the existence of spatially heterogeneous solutions, most focus on one-dimensional domains or simplified models, leaving open the problem of rigorous higher-dimensional analysis. This work addresses that gap by extending the framework of [39] to higher dimensions and by developing a general approach for bifurcation analysis in three-agent systems on spatial domains. To do so, the paper follows the framework presented in [8], where bifurcation analysis was

https://doi.org/10.1017/S0956792526100357 Published online by Cambridge University Press

done on a two-component system (1.1.1). Essentially, this paper should be viewed as a convergence of two works [8, 39], extending in both the number of components and the dimension of the underlying geometry. We establish the Crandall–Rabinowitz theorem and stability results for systems with guardians in any spatial dimension, using Laplacian eigenvalues rather than wave-mode numbers (Theorems 2.2, 3.1). Our proofs are given in explicit detail, making the methods adaptable to other three-agent systems. We also generalize the Hopf bifurcation theorem to higher dimensions [1] (Theorem 4.1). On the computational side, we provide parameter-based verification guided by linear stability analysis and include simulations in both one- and two-dimensional dimensions. These simulations highlight features such as long transients and consistent behaviours across dimensions. We further demonstrate chaotic dynamics using bifurcation diagrams and perform a systematic parameter sweep to explore how parameter magnitudes affect system outcomes. Together, these results provide a comprehensive and general treatment of the target–guardian–offender model.

This work develops its analysis through three sequential components: first, a linear stability examination of the constant solution (SS) establishes the baseline conditions for pattern formation; second, a steady state bifurcation analysis reveals how intensive guardians drive the emergence of nontrivial solutions from this trivial state and third, a Hopf bifurcation analysis locating the onset of oscillatory behaviour and proving the existence of periodic solutions. Finally, we complement our theoretical results with numerical simulations that not only validate our predictions but also reveal complex, chaotic dynamics. These simulations highlight the rich pattern formation potential of the extended system and demonstrate behaviours not previously captured in earlier models.

2. Steady state bifurcation analysis

In this section, we perform a bifurcation analysis to demonstrate the existence of non-constant steady-state solutions, thereby showing that the system can generate stable spatial patterns under suitable conditions. The main idea is to translate the problem into an equivalent linear algebra setting and carry out the analysis there. In [10], this approach is applied to a two–component system, where the corresponding algebra is simpler; for instance, the determinant of a 2×2 matrix has a closed-form expression, unlike the 3×3 case considered here. Following the framework of [10], we emphasize the additional steps needed to address these higher–dimensional algebraic challenges.

For the sake of simplicity, we shift the scalar fields in system (E) using the steady state (SS) by setting

$$\tilde{A}(\mathbf{x}, t) := A(\mathbf{x}, t) - \bar{A}, \quad \tilde{\rho}(\mathbf{x}, t) := \rho - \bar{\rho}, \quad \tilde{u}(\mathbf{x}, t) := u(\mathbf{x}, t) - \bar{u}.$$

and collect the following the equivalent system for $(\bar{A}, \bar{\rho}, \bar{u})$

$$\begin{cases} \dfrac{\partial \tilde{A}}{\partial t} = D_A \Delta \tilde{A} - \tilde{A} + \tilde{A}\tilde{\rho} + \bar{\rho}\tilde{A} + \bar{A}\tilde{\rho} + \bar{A}\bar{\rho} + \alpha, & \text{in } \Omega \times (0, T], \\ \dfrac{\partial \tilde{\rho}}{\partial t} = \nabla \cdot (D_\rho \nabla \tilde{\rho} - \dfrac{2(\tilde{\rho} + \bar{\rho})}{\tilde{A} + \bar{A}} \nabla \tilde{A}) \\ \qquad - \tilde{A}\tilde{\rho} - \bar{A}\tilde{\rho} - \bar{\rho}\tilde{A} - \tilde{\rho}\tilde{u} - \bar{u}\tilde{\rho} - \bar{\rho}\tilde{u} + \beta - \bar{\rho}(\bar{u} + \bar{A}), & \text{in } \Omega \times (0, T], \\ \dfrac{\partial \tilde{u}}{\partial t} = \nabla \cdot \left(D_u \nabla \tilde{u} - \dfrac{\chi(\tilde{u} + \bar{u})}{\tilde{A} + \bar{A}} \nabla \tilde{A} \right), & \text{in } \Omega \times (0, T], \\ \dfrac{\partial \tilde{A}}{\partial \mathbf{n}} = \dfrac{\partial \tilde{\rho}}{\partial \mathbf{n}} = \dfrac{\partial \tilde{u}}{\partial \mathbf{n}} = 0, & \text{on } \partial\Omega. \end{cases} \tag{ME}$$

https://doi.org/10.1017/S0956792526100357 Published online by Cambridge University Press

This new system (ME) has a shifted equilibrium $\mathbf{0} := (0,0,0)$, and dropping tildes we obtain

$$\begin{cases} \dfrac{\partial A}{\partial t} = D_A \Delta A - A + A\rho + \left(1 - \dfrac{\alpha}{\lambda}\right) A + \lambda\rho, & \text{in } \Omega \times (0,T], \\ \dfrac{\partial \rho}{\partial t} = \nabla \cdot \left(D_\rho \nabla \rho - \dfrac{2\left(\rho + \left(1 - \frac{\alpha}{\lambda}\right)\right)}{A+\lambda} \nabla A \right) - A\rho - \lambda\rho \\ \qquad\qquad - \left(1 - \dfrac{\alpha}{\lambda}\right) A - \rho u - \rho\lambda \left(\dfrac{\beta}{\lambda - \alpha} - 1 \right) - u \left(1 - \dfrac{\alpha}{\lambda}\right), & \text{in } \Omega \times (0,T], \\ \dfrac{\partial u}{\partial t} = \nabla \cdot \left(D_u \nabla u - \dfrac{\chi \left(u + \lambda \left(\frac{\beta}{\lambda - \alpha} - 1\right)\right)}{A+\lambda} \nabla A \right), & \text{in } \Omega \times (0,T], \\ \dfrac{\partial A}{\partial \mathbf{n}} = \dfrac{\partial \rho}{\partial \mathbf{n}} = \dfrac{\partial u}{\partial \mathbf{n}} = 0, & \text{on } \partial\Omega. \end{cases} \tag{MP}$$

We now aim to study the steady-state solutions of system (MP), and to this end, we introduce the operator $\mathcal{F}$ as follows

$$\begin{aligned} &\mathcal{F}(\chi, A, \rho, u) \\ &:= \begin{bmatrix} D_A \Delta A + A\rho - \frac{\alpha}{\lambda} A + \lambda\rho \\ \nabla \cdot \left[D_\rho \nabla \rho - \frac{2\left(\rho + \left(1 - \frac{\alpha}{\lambda}\right)\right)}{A+\lambda} \nabla A \right] - A\rho - \lambda\rho - \left(1 - \frac{\alpha}{\lambda}\right) A - \rho u - \rho\lambda \left(\frac{\beta}{\lambda - \alpha} - 1 \right) - u \left(1 - \frac{\alpha}{\lambda}\right) \\ \nabla \cdot \left[D_u \nabla u - \frac{\chi \left(u + \lambda \left(\frac{\beta}{\lambda - \alpha} - 1\right)\right)}{A+\lambda} \nabla A \right] \end{bmatrix}. \end{aligned} \tag{2.0.1}$$

Then, $\mathcal{F}(\chi, \mathbf{0}) = 0$ for any $\chi \in \mathbb{R}$, and we are motivated to find nontrivial equilibria of (MP) that bifurcate from the trivial one. It is equivalent to solving the following problem

$$\mathcal{F}(\chi, A, \rho, u) = 0, \quad \chi \in \mathbb{R}, \quad (A, \rho, u) \in \mathcal{Y}, \tag{EP}$$

where

$$\mathcal{Y} = \left\{ (A, \rho, u) \in [H^2(\Omega)]^3 \,\middle|\, \frac{\partial A}{\partial \mathbf{n}} = \frac{\partial \rho}{\partial \mathbf{n}} = \frac{\partial u}{\partial \mathbf{n}} = 0 \text{ on } \partial\Omega, \ \int_\Omega u d\mathbf{x} = 0 \right\}.$$

Indeed, any root of $\mathcal{F} = 0$ is known to be a weak solution of (2.0.1), and standard elliptic regularity theory then ensures that this weak solution is, in fact, classical and smooth.

We now state the main bifurcation theorem used in this section. The original local result is due to Crandall and Rabinowitz [10, Theorem 1.7], and it was later extended to a global bifurcation result in [45, Theorem 4.3]. Part (e), while not stated explicitly in either theorem, concerns the global continuation and the Fredholm property of the linearized operator. For full details, we refer the reader to these references. Here, we present a version adapted to our setting; see also [8].

Theorem 2.1. *Let $\mathcal{Y}$ and $\mathcal{Z}$ be real Banach spaces and $\mathcal{V}$ be an open set in $\mathbb{R} \times \mathcal{Y}$ such that $(\chi_0, 0) \in \mathcal{V}$ for some χ_0. Let $\mathcal{F} : \mathcal{V} \to \mathcal{Z}$ be such that $\mathcal{F}$ is continuously differentiable and satisfies the following*

(a) $\mathcal{F}(\chi, 0) = 0$ for all $(\chi, 0) \in \mathcal{V}$;

(b) $D\mathcal{F}_{\chi y}(\chi, y)$ exists and is continuous;

(c) $ran(D\mathcal{F}_y(\chi_0, 0))$ is closed $\dim \ker (D\mathcal{F}_y(\chi_0, 0)) = 1$, *and* $codimran(D\mathcal{F}_y(\chi_0, 0)) = 1$;

(d) $D\mathcal{F}_{\chi y}(\chi_0, 0) y_0 \notin ran(D\mathcal{F}_y(\chi_0, 0))$, where y_0 spans $\ker (D\mathcal{F}_y(\chi_0, 0))$.

Let $\mathcal{W} \subset \mathcal{Y}$ be any closed complement of $span(y_0)$. Then, there exists an open interval $\mathcal{I}_0$ containing 0 and continuously differentiable functions $\chi : \mathcal{I}_0 \to \mathbb{R}$ and $\xi : \mathcal{I}_0 \to \mathcal{W}$ with $\chi(0) = \chi_0$, $\xi(0) = 0$, such

https://doi.org/10.1017/S0956792526100357 Published online by Cambridge University Press

that $\mathcal{F}(\chi(s), sy_0 + s\xi(s)) = 0$ for $s \in \mathcal{I}_0$. In addition, the entire solution set for $\mathcal{F}(\chi, y) = 0$ in any sufficiently small neighbourhood of $(\chi, 0)$ in $\mathcal{V}$ consists of the line $(\chi, 0)$ and the curve $(\chi(s), sy_0 + s\xi(s))$. Furthermore, if

(e) $D\mathcal{F}_y(\chi, 0)$ is a Fredholm operator for all $(\chi, y) \in \mathcal{V}$,

then the curve $(\chi(s), sy_0 + s\xi(s))$ is contained in $\mathcal{C}$, which is a connected component of $\bar{\mathcal{S}}$, where $\mathcal{S} = \{(\chi, y) \in \mathcal{V} : \mathcal{F}(\chi, y) = 0, y \neq 0\}$ and either $\mathcal{C}$ is not compact in $\mathcal{V}$ or $\mathcal{C}$ contains a point $(\chi^*, 0)$ with $\chi^* \neq \chi_0$.

We will show that the conditions of Theorem 2.1 are satisfied for $\mathcal{F} = F$ in (EP), $\mathcal{Y} = Y$, $\mathcal{Z} = Z$ and $\mathcal{V} = V$ defined as follows

$$V = \left\{ (\chi, A, \rho, u) \in \mathbb{R} \times \mathcal{Y} |\, A > -\lambda,\ \rho > \frac{\alpha}{\lambda} - 1,\ u > \lambda \left(1 - \frac{\beta}{\lambda - \alpha}\right) \right\},$$

and $Z := [L^2(\Omega)]^3$.

Now that $\mathcal{F}(\chi, \mathbf{0}) = 0$ holds for all $\chi \in \mathbb{R}$, to look for nonconstant solutions, one first needs the implicit function theorem to fail at this trivial location. For this purpose, we consider the following eigenvalue problem

$$\Delta\phi + \mu\phi = 0 \text{ in } \Omega, \text{ with } \partial_{\mathbf{n}}\phi = 0 \text{ on } \partial\Omega \quad \text{and } \|\phi\|_{L^2(\Omega)} = 1. \tag{LN}$$

It is well known that its eigen pairs $< \mu_j, \phi_j >$ consist of a sequence of real, non-negative and diverging eigenvalues:

$$0 = \mu_0 < \mu_1 \leq \mu_2 \leq \ldots \to \infty,$$

and the eigenfunction set $\{\phi_j\}_{j=0}^{\infty} \subset H^1(\Omega)$ form a complete orthonormal basis of $L^2(\Omega)$. To apply the bifurcation from simple eigenfunctions, we assume that μ has algebraic multiplicity one. Then, y_0 in Theorem 2.1 is relabelled as $\mathbf{P}(\mathbf{x})$ and defined as follows

$$\mathbf{P}(\mathbf{x}) = \left(1, \frac{1}{\lambda}\left(D_A\mu + \frac{\alpha}{\lambda}\right), \frac{(2\mu - \lambda)(\lambda - \alpha)^2 - (D_A\lambda\mu + \alpha)(D_\rho\mu(\lambda - \alpha) + \beta\lambda)}{\lambda(\lambda - \alpha)^2}\right)\phi(\mathbf{x}). \tag{2.0.2}$$

The associated linear functional on Y is then

$$\ell\varphi = \int_\Omega \varphi \cdot \mathbf{P}(\mathbf{x}),$$

which allows us to define the closed complement $\mathcal{W} = W$

$$W = \{\varphi \in Y | \ell\varphi = 0\}.$$

Using the definitions above and Theorem 1.7 in [10], we extend Theorems 2.2 and 2.6 in [8] as follows.

Theorem 2.2. *Let $\mu > 0$ be a generic and simple eigenvalue of (LN). Denote*

$$\chi = \overbrace{-\frac{D_u}{(\beta + \alpha - \lambda)}\left[\left(\lambda - \alpha + \frac{\alpha\beta}{\lambda - \alpha}\right) + \mu\left(-2\left(1 - \frac{\alpha}{\lambda}\right) + \frac{D_\rho\alpha}{\lambda} + \frac{D_A\beta\lambda}{\lambda - \alpha}\right) + \mu^2 D_A D_\rho\right]}^{\triangleq \chi_0} \tag{2.0.3}$$

and assume that

$$\frac{(D_u - \chi_0)(\alpha^2 + \alpha(\beta - 2\lambda) + \lambda^2) - \beta\lambda\chi_0}{\mu(\lambda - \alpha)}$$

is not eigenvalue of (LN). Then, a branch of spatially nonconstant solutions of $\mathcal{F}$ bifurcates from the equilibrium $(\bar{A}, \bar{\rho}, \bar{u})$ at $\chi = \chi_0$. In a neighbourhood of the bifurcation point, the bifurcating branch can be parametrized as $(A, \rho, u)(\boldsymbol{x}; s) = (\bar{A}, \bar{\rho}, \bar{u}) + s\boldsymbol{P}(\boldsymbol{x}) + s^2\boldsymbol{Q}(\boldsymbol{x}; s)$ with $\boldsymbol{P}$ given by (2.0.2) and $\boldsymbol{Q}(\boldsymbol{x}; s) \in W$ for any $s \in (-\epsilon, \epsilon)$, and $\chi(0) = \chi_0$. Furthermore, the bifurcation branch is part of a connected component $\mathcal{C}$ of the set $\bar{\mathcal{S}}$, where $\mathcal{S} = \{(\chi, A, \rho, u) : (\chi, A - \bar{A}, \rho - \bar{\rho}, u - \bar{u}) \in V \mid \mathcal{F}(\chi, A - \bar{A}, \rho - \bar{\rho}, u - \bar{u}) = 0, (A, \rho, u) \neq (\bar{A}, \bar{\rho}, \bar{u})\}$, and $\mathcal{C}$ either is not compact or contains point $(\chi^*, \bar{A}, \bar{\rho}, \bar{u})$ with $\chi^* \neq \chi_0$.

https://doi.org/10.1017/S0956792526100357 Published online by Cambridge University Press

Remark 2.1. In [8], the authors showed that if $\mathcal{C}$ is not compact, then it must be unbounded (see Remark 2.4). This implies that $\mathcal{C}$ either extends to infinity in one of the parameters χ, A, ρ, or u, or else leaves V, in which case $\mathcal{C}$ contains a point on ∂V. This conclusion, established in their Lemma 2.5, relies on the theory developed in [26]. The same lemma and conclusion can be applied, here; the only distinction is that we must additionally show that u is uniformly bounded in $C^{2,\vartheta}(\bar{\Omega})$. However, the proof of this step is identical to the argument used for ρ in [8].

Mathematically, the value χ_0 marks the point at which the homogeneous steady state loses stability and new nontrivial steady states emerge through bifurcation. From a criminological perspective, this corresponds to a tipping point in policing intensity: below $\chi_0 > 0$, police and offenders distribute uniformly in space; however, once χ_0 is exceeded, stable, spatially inhomogeneous patterns arise, which may manifest as persistent crime hotspots despite ongoing policing efforts. This seems counterintuitive. However, one could explain this by noting that high concentrations of u may lead to a local decrease in ρ and A, thereby displacing these scalar fields elsewhere. Then, u would follow the gradient, displacing hotspots again. In this way, one can obtain temporally varying solutions as well. At the same time, such a paradox may highlight the modelling limitations of the system and call for further refinement. There is also another explanation, as we unravel the expression for χ_0. For a fixed μ, which essentially represents geometry, the positivity of χ_0 is dependent on the coefficient in front of μ in (2.0.3). χ_0 is proportional to D_u. Hence, more police "spread" requires more "concentrated movement" to generate a pattern and vice versa. Thus, to eliminate any clusters, the police agents need to increase their diffusion or lower their concentration intensity. The relationship between χ_0 and other parameters is more convoluted, but one could observe that higher values of D_A and D_ρ would lead to the fact that there is no $\mu > 0$ for which $\chi_0 > 0$. Thus, again, patterns cannot be formed at least from the initial constant steady state. The relationship will be more illustrative in the later chapter, where we perform numerical simulations and parameter explorations.

2.1. Identification of bifurcation points

To apply the Crandall–Rabinowitz bifurcation theory [10, 45], we first note that $\mathcal{F}$ is Fréchet differentiable and its functional derivative at (A, ρ, u) with $\mathbf{v} := (v_1, v_2, v_3)$ is given by

$$
\begin{aligned}
&D\mathcal{F}_{(A,\rho,u)}(\chi, A, \rho, u)[\mathbf{v}] \\
&= \begin{bmatrix}
D_A \Delta v_1 + \left(\rho - \frac{\alpha}{\lambda}\right) v_1 + (A + \lambda)\, v_2 \\
\nabla \cdot \left[D_\rho \nabla v_2 - \frac{2v_2}{A+\lambda} \nabla A - 2\left(\rho + 1 - \frac{\alpha}{\lambda}\right) \left(\frac{\nabla v_1}{A+\lambda} - \frac{v_1 \nabla A}{(A+\lambda)^2} \right) \right] \\
-\left(\rho + 1 - \frac{\alpha}{\lambda}\right) v_1 - \left(A + u + \frac{\lambda\beta}{\lambda - \beta}\right) v_2 - \left(\rho + 1 - \frac{\alpha}{\lambda}\right) v_3 \\
\nabla \cdot \left[D_u \nabla v_3 - \frac{\chi v_3}{A+\lambda} \nabla A - \chi \left(u + \lambda \left(\frac{\beta}{\lambda - \alpha} - 1 \right) \right) \left(\frac{\nabla v_1}{A+\lambda} - \frac{v_1 \nabla A}{(A+\lambda)^2} \right) \right]
\end{bmatrix}.
\end{aligned}
\tag{2.1.1}
$$

One can continue to show that $\frac{d}{d\chi} D\mathcal{F}_{(A,\rho,u)}(\chi, A, \rho, u)[\mathbf{v}]$ exists and is continuous. To fail the implicit function theorem at $(\chi, \mathbf{0})$, we evaluate (2.1.1) the following way

$$
\begin{aligned}
&D\mathcal{F}_{(A,\rho,u)}(\chi, \mathbf{0})[\mathbf{v}] \\
&= \begin{bmatrix}
D_A \Delta v_1 - \frac{\alpha}{\lambda} v_1 + \lambda v_2 \\
D_\rho \Delta v_2 - \frac{2}{\lambda} \left(1 - \frac{\alpha}{\lambda}\right) \Delta v_1 - \left(1 - \frac{\alpha}{\lambda}\right) v_1 - \frac{\lambda\beta}{\lambda - \alpha} v_2 - \left(1 - \frac{\alpha}{\lambda}\right) v_3 \\
D_u \Delta v_3 - \chi \left(\frac{\beta}{\lambda - \alpha} - 1 \right) \Delta v_1
\end{bmatrix}.
\end{aligned}
\tag{2.1.2}
$$

https://doi.org/10.1017/S0956792526100357 Published online by Cambridge University Press

Then we are to look for nontrivial solutions of the following equation

$$\begin{cases} D_A\Delta v_1 - \dfrac{\alpha}{\lambda}v_1 + \lambda v_2 = 0, & \text{in } \Omega, \\ D_\rho\Delta v_2 - \dfrac{2}{\lambda}\left(1-\dfrac{\alpha}{\lambda}\right)\Delta v_1 - \left(1-\dfrac{\alpha}{\lambda}\right)v_1 - \dfrac{\lambda\beta}{\lambda-\alpha}v_2 - \left(1-\dfrac{\alpha}{\lambda}\right)v_3 = 0, & \text{in } \Omega, \\ D_u\Delta v_3 - \chi\left(\dfrac{\beta}{\lambda-\alpha}-1\right)\Delta v_1 = 0, & \text{in } \Omega, \\ \dfrac{\partial v_1}{\partial \mathbf{n}} = \dfrac{\partial v_2}{\partial \mathbf{n}} = \dfrac{\partial v_3}{\partial \mathbf{n}} = 0, & \text{on } \partial\Omega. \end{cases} \tag{LE}$$

We test each equation with ϕ and then apply integration by parts to obtain

$$\overbrace{\begin{bmatrix} -D_A\mu - \frac{\alpha}{\lambda} & \lambda & 0 \\ \left(\frac{2\mu}{\lambda}-1\right)\left(1-\frac{\alpha}{\lambda}\right) & -D_\rho\mu - \frac{\beta\lambda}{\lambda-\alpha} - \left(1-\frac{\alpha}{\lambda}\right) & \\ \mu\chi\left(\frac{\beta}{\lambda-\alpha}-1\right) & 0 & -D_u\mu \end{bmatrix}}^{\triangleq H} \begin{bmatrix} \int_\Omega v_1\phi \\ \int_\Omega v_2\phi \\ \int_\Omega v_3\phi \end{bmatrix} = \begin{bmatrix} 0 \\ 0 \\ 0 \end{bmatrix}. \tag{2.1.3}$$

Then the existence of nontrivial solutions of (LE) will in turn give us nontrivial solutions for (2.1.3), where H is such that $\int_\Omega D\mathcal{F}_{(A,\rho,u)}(\chi,\mathbf{0})[\phi\mathbf{v}] = H\int_\Omega \phi\mathbf{v}$. That said, matrix H must be non-invertible such that

$$-D_u\mu\left(D_A\mu+\frac{\alpha}{\lambda}\right)\left(D_\rho\mu+\frac{\beta\lambda}{\lambda-\alpha}\right) + D_u\lambda\mu\left(\frac{2\mu}{\lambda}-1\right)\left(1-\frac{\alpha}{\lambda}\right) - \lambda\mu\chi\left(1-\frac{\alpha}{\lambda}\right)\left(\frac{\beta}{\lambda-\alpha}-1\right) = 0$$

or equivalently when χ is given by (2.0.3).

This analysis identifies the critical bifurcation values of χ, representing the policing intensity, that mark the transition from homogeneous to patterned states, as determined by the linear stability analysis of the constant solution (SS). Moreover, when $\chi = \chi_0$, it follows directly from (2.1.3) that the kernel of $D\mathcal{F}(\chi_0,\mathbf{0})$ is one-dimensional and is spanned by $\mathbf{P}$ defined in (2.0.2).

To proceed further, we verify Agmon's condition following [8, 45]. Define the principal part of the elliptic operator $F(\chi,A,\rho,u)$ and $D\mathcal{F}_{(A,\rho,u)}(\chi,A,\rho,u)$

$$A_1(\chi,A,\rho,u) = \begin{bmatrix} D_A & 0 & 0 \\ -2\frac{\rho+\left(1-\frac{\alpha}{\lambda}\right)}{A+\lambda} & D_\rho & 0 \\ -\chi\frac{u+\lambda\left(\frac{\beta}{\lambda-\alpha}-1\right)}{A+\lambda} & 0 & D_\rho \end{bmatrix}.$$

More importantly, we need to look at the determinant $A_1(\chi,A,\rho,u)+\sigma I$, $\sigma\in\mathbb{C}$

$$\begin{vmatrix} D_A+\sigma & 0 & 0 \\ -2\frac{\rho+\left(1-\frac{\alpha}{\lambda}\right)}{A+\lambda} & D_\rho+\sigma & 0 \\ -\chi\frac{u+\lambda\left(\frac{\beta}{\lambda-\alpha}-1\right)}{A+\lambda} & 0 & D_u+\sigma \end{vmatrix} = (D_A+\sigma)(D_\rho+\sigma)(D_u+\sigma).$$

The later is nonzero when $\sigma=0$ or $\arg\sigma\in[-\pi/2,\pi/2]$. This, in turn, implies that the operator $D\mathcal{F}_{(A,\rho,u)}(\chi,A,\rho,u)$ is a Fredholm operator with index 0 and $\mathrm{ran}(D\mathcal{F}_{(A,\rho,u)}(\chi_0,\mathbf{0}))$ has a codimension of 1.

https://doi.org/10.1017/S0956792526100357 Published online by Cambridge University Press

2.2. Transversality and steady-state bifurcation

We now verify that bifurcation does occur at χ_0 given by (2.0.3) by proving the following transversality condition

$$\frac{d}{d\chi}D\mathcal{F}_{(A,\rho,u)}(\chi_0,\mathbf{0})[\mathbf{P}(\mathbf{x})] \notin \operatorname{ran}(D\mathcal{F}_{(A,\rho,u)}(\chi_0,\mathbf{0})).$$

We argue by contradiction and assume that there exists nonzero $\hat{\mathbf{v}} := (\hat{v}_1, \hat{v}_2, \hat{v}_3)$ such that

$$D\mathcal{F}_{(A,\rho,u)}(\chi,\mathbf{0})[\hat{\mathbf{v}}] = \frac{d}{d\chi}D\mathcal{F}_{(A,\rho,u)}(\chi,\mathbf{0})[\mathbf{P}(\mathbf{x})].$$

Since

$$\frac{d}{d\chi}D\mathcal{F}_{(A,\rho,u)}(\chi_0,\mathbf{0})[\mathbf{P}(\mathbf{x})] = \begin{bmatrix} 0 \\ 0 \\ \mu\left(\frac{\beta}{\lambda-\alpha}-1\right)\phi \end{bmatrix},$$

we collect the following system

$$\begin{cases} D_A\Delta\hat{v}_1 - \dfrac{\alpha}{\lambda}\hat{v}_1 + \lambda\hat{v}_2 = 0, & \text{in } \Omega, \\ D_\rho\Delta\hat{v}_2 - \dfrac{2}{\lambda}\left(1-\dfrac{\alpha}{\lambda}\right)\Delta\hat{v}_1 - \left(1-\dfrac{\alpha}{\lambda}\right)\hat{v}_1 - \dfrac{\lambda\beta}{\lambda-\alpha}\hat{v}_2 - \left(1-\dfrac{\alpha}{\lambda}\right)\hat{v}_3 = 0, & \text{in } \Omega, \\ D_u\Delta\hat{v}_3 - \chi_0\left(\dfrac{\beta}{\lambda-\alpha}-1\right)\Delta\hat{v}_1 = \mu\left(\dfrac{\beta}{\lambda-\alpha}-1\right)\phi, & \text{in } \Omega, \\ \dfrac{\partial\hat{v}_1}{\partial\mathbf{n}} = \dfrac{\partial\hat{v}_2}{\partial\mathbf{n}} = \dfrac{\partial\hat{v}_3}{\partial\mathbf{n}} = 0, & \text{on } \partial\Omega. \end{cases} \tag{S_1}$$

We test (S_1) by ϕ and then collect the following identity using the fact that $\|\phi\|_{L^2} = 1$

$$\begin{bmatrix} -D_A\mu - \frac{\alpha}{\lambda} & \lambda & 0 \\ \left(\frac{2\mu}{\lambda}-1\right)\left(1-\frac{\alpha}{\lambda}\right) & -D_\rho\mu - \frac{\beta\lambda}{\lambda-\alpha} - \left(1-\frac{\alpha}{\lambda}\right) & \\ \mu\chi_0\left(\frac{\beta}{\lambda-\alpha}-1\right) & 0 & -D_u\mu \end{bmatrix} \begin{bmatrix} \int_\Omega \hat{v}_1\phi \\ \int_\Omega \hat{v}_2\phi \\ \int_\Omega \hat{v}_3\phi \end{bmatrix} = \begin{bmatrix} 0 \\ 0 \\ \mu\left(\frac{\beta}{\lambda-\alpha}-1\right) \end{bmatrix}.$$

However, this reaches a contradiction to (2.1.3) since H therein is non-invertible with $\chi = \chi_0$. This verifies the transversality condition, and Theorem 2.2 follows from those in [10].

3. Stability analysis of the bifurcating steady states

In this section, we establish conditions for the stability of spatially heterogeneous patterns. Unlike previous analyses, our approach explicitly incorporates the geometry of the domain. Nevertheless, the results remain applicable to a broad class of domains, including discs. Compared to [8], the algebra in our setting is more involved because it includes cubic polynomials. We carefully work through these terms to obtain a general result. To this end, we introduce the following cubic equation in σ, which is a characteristic equation of matrix H in (2.1.3) The characteristic equation is given as:

$$\sigma^3 + a_2(\mu)\sigma^2 + a_1(\mu)\sigma^1 + a_0(\mu,\chi) = 0, \tag{3.0.1}$$

https://doi.org/10.1017/S0956792526100357 Published online by Cambridge University Press

where

$$
\begin{aligned}
a_2(\mu) &:= \frac{\alpha}{\lambda} + \frac{\beta\lambda}{\lambda-\alpha} + \mu\left(D_A + D_\rho + D_u\right),\\
a_1(\mu) &:= (\lambda-\alpha) + \frac{\alpha\beta}{\lambda-\alpha} + \mu\left[-2\left(1-\frac{\alpha}{\lambda}\right) + \frac{D_\rho\alpha}{\lambda} + \frac{D_A\beta\lambda}{\lambda-\alpha} + D_u\left(\frac{\beta\lambda}{\lambda-\alpha} + \frac{\alpha}{\lambda}\right)\right]\\
&\quad + \mu^2\left(D_AD_\rho + D_AD_u + D_\rho D_u\right),\\
a_0(\mu,\chi) &:= D_u\mu\left\{-\left[\mu_*\left(-2\left(1-\frac{\alpha}{\lambda}\right) + \frac{D_\rho\alpha}{\lambda} + \frac{D_A\beta\lambda}{\lambda-\alpha}\right) + \mu_*^2 D_AD_\rho\right]\right.\\
&\quad \left. + \mu\left[-2\left(1-\frac{\alpha}{\lambda}\right) + \frac{D_\rho\alpha}{\lambda} + \frac{D_A\beta\lambda}{\lambda-\alpha}\right] + \mu^2 D_AD_\rho\right\}. \qquad (3.0.2)
\end{aligned}
$$

We are going to explore when the eigenvalues of H have positive real parts. We will apply Routh–Hurwitz criterion, where we need to look at the polynomial equation $a_2(\mu)a_1(\mu) - a_0(\mu,\chi) = 0$

$$
\begin{aligned}
0 &= \mu^0\left\{\left(\frac{\alpha}{\lambda} + \frac{\beta\lambda}{\lambda-\alpha}\right)\left[(\lambda-\alpha) + \frac{\alpha\beta}{\lambda-\alpha}\right]\right\} + \mu^1\left\{\left(D_A + D_\rho + D_u\right)\left((\lambda-\alpha) + \frac{\alpha\beta}{\lambda-\alpha}\right)\right.\\
&\quad + \left(\frac{\alpha}{\lambda} + \frac{\beta\lambda}{\lambda-\alpha}\right)\left[-2\left(1-\frac{\alpha}{\lambda}\right) + \frac{D_\rho\alpha}{\lambda} + \frac{D_A\beta\lambda}{\lambda-\alpha} + D_u\left(\frac{\beta\lambda}{\lambda-\alpha} + \frac{\alpha}{\lambda}\right)\right]\\
&\quad \left. + \mu_*\left[\left(-2\left(1-\frac{\alpha}{\lambda}\right) + \frac{D_\rho\alpha}{\lambda} + \frac{D_A\beta\lambda}{\lambda-\alpha}\right) + \mu_* D_AD_\rho\right]\right\}\\
&\quad + \mu^2\left\{\left(D_A + D_\rho\right)\left[-2\left(1-\frac{\alpha}{\lambda}\right) + \frac{D_\rho\alpha}{\lambda} + \frac{D_A\beta\lambda}{\lambda-\alpha}\right] + \left[\left(D_A + D_\rho + D_u\right)\left(\frac{\beta\lambda}{\lambda-\alpha} + \frac{\alpha}{\lambda}\right)\right]\right.\\
&\quad \left. + \left(\frac{\alpha}{\lambda} + \frac{\beta\lambda}{\lambda-\alpha}\right)\left(D_AD_\rho + D_AD_u + D_\rho D_u\right)\right\}\\
&\quad + \mu^3\left\{\left(D_A + D_\rho\right)\left(D_A + D_u\right)\left(D_\rho + D_u\right)\right\}\\
&= C\left(\mu-\mu_1\right)\left(\mu-\mu_2\right)\left(\mu-\mu_3\right), \qquad (3.0.3)
\end{aligned}
$$

where μ_i denote the roots of (3.0.3). At least one of these roots must be negative; without loss of generality, we denote this root by μ_3. With this set-up, we are ready to state the next result.

Theorem 3.1. *Suppose that μ is the eigenvalue of $-\Delta$ appearing in Theorem 2.2 with normalized eigenfunction ϕ. Suppose that the hypotheses of Theorem 2.2 are satisfied. Assume that $\int_\Omega \phi^3 \neq 0$ and $\beta \neq -C_2/C_1$, where*

$$
\begin{aligned}
C_1 &= -\lambda\left(\chi_0 - D_u\right)\left(-\alpha\chi_0 + 2D_AD_u\lambda\mu + 2D_u\alpha + \lambda\chi_0\right),\\
C_2 &= -(\lambda-\alpha)\left\{\lambda\left[-2D_u^2\mu\left(D_A(\mu D_\rho - \lambda + \mu) - 1\right) + D_u\lambda\chi_0(1 - 2\mu D_A) - \lambda\chi_0^2\right]\right.\\
&\quad \left. + \alpha\left[2D_u^2\left(\lambda - \mu(D_\rho + 2)\right) - 3D_u\lambda\chi_0 + \lambda\chi_0^2\right]\right\}.
\end{aligned}
$$

Suppose that there are no eigenvalue of $-\Delta$, ν, such that $(\max\{0, \theta-\mu\} < \nu < \max\{\mu, \theta-\mu\})$, *where*

$$
\theta = \frac{2\lambda(\lambda-\alpha) - \alpha(\lambda-\alpha)(2+D_\rho) - D_A\beta\lambda^2}{D_AD_\rho\lambda(\lambda-\alpha)}.
$$

https://doi.org/10.1017/S0956792526100357 Published online by Cambridge University Press

If μ_1 and μ_2 are both positive roots of (3.0.3), further suppose that, μ (and $\theta-\mu$ in case it is an eigenvalue of $-\Delta$) are outside of the interval $(\min\{\mu_1,\mu_2\},\max\{\mu_1,\mu_2\})$. *Then the branch* $(\chi(s),A(s),\rho(s),u(s))$ *of solution of (EQ) bifurcating from* $(\chi_0,\bar{A},\bar{\rho},\bar{u})$ *is stable for sufficiently small and non-zero* $|s|$.

Proof. We proceed by following the approach outlined in [8], where the authors apply the bifurcation theory developed in [11]. The stability of the bifurcation branch $(\chi(s),A(s),\rho(s),u(s))$ of (EP) (or equivalently (EQ), by translation) is determined by the eigenvalues of $D\mathcal{F}(A,\rho,u)(\chi(s),A(s),\rho(s),u(s))$. In particular, the branch is stable if all eigenvalues have negative real parts. Theorem 2.2 implies that $D\mathcal{F}(A,\rho,u)(\chi_0,\mathbf{0})$ has 0 as an i-simple eigenvalue, where i is an injection. Moreover, Corollary 1.13 in [11] ensures the existence of intervals I and J with $\chi_0\in I$ and $0\in J$, together with continuously differentiable functions $\gamma:I\to\mathbb{R}$, $\sigma:J\to\mathbb{R}$, $[\mathbf{v}]:I^3\to Y$ and $(w_1,w_2,w_3):J^3\to Y$ such that

$$D\mathcal{F}_{(A,\rho,u)}(\chi,\mathbf{0})[\mathbf{v}]^T=\gamma(\chi)[\mathbf{v}]^T,$$

$$D\mathcal{F}_{(A,\rho,u)}(\chi(s),A(s),\rho(s),u(s))(w_1,w_2,w_3)^T=\sigma(s)(w_1,w_2,w_3)^T,$$

such that

$$\chi(0)=\chi_0,\quad \gamma(\chi_0)=\sigma(0)=0,\quad (v_1(\chi_0),v_2(\chi_0),v_3(\chi_0))=(w_1(0),w_2(0),w_3(0))=\mathbf{P}(\mathbf{x}),$$

$$(v_1(\chi),v_2(\chi),v_3(\chi))-\mathbf{P}(\mathbf{x})\in W,\quad (w_1(s),w_2(s),v_3(s))-\mathbf{P}(\mathbf{x})\in W.$$

Theorem 1.16 in [11] states that under the assumptions and definitions of Corollary 1.13, $\sigma(s)$ has only zero at $s=0$ and the same sign as s for $|s|>0$ for sufficiently small $|s|$ and whenever $\chi'(0)\neq 0$. It follows that if $\gamma(\chi_0)=\sigma(0)$ is the eigenvalue of (2.0.1) with the largest real part at $(\chi_0,\mathbf{0})$, then again for sufficiently small nonzero s, $\sigma(s)$ is eigenvalue of the linearization of (2.0.1) at $(\chi(s),A(s),\rho(s),u(s))$ with the largest real part. In particular, if $\mathcal{R}e(\sigma(0))<0$, then $\mathcal{R}e(\sigma(s))<0$.

Hence, it remains to show that, under assumptions of Theorem 3.1, (a) $\chi'(0)\neq 0$, and (b) $\sigma(0)=0$ is the largest eigenvalue of the linearized operator $D\mathcal{F}_{(A,\rho,u)}(\chi,A,\rho,u)$ at $(\chi_0,\mathbf{0})$.

To this end, we write system (EP) with the bifurcating solution as

$$\mathcal{F}(\chi(s),A(s),\rho(s),u(s))=0,$$

with $\mathbf{x}$ omitted for notational simplicity. We then differentiate twice with respect to s at $s=0$ to obtain.

$$D_A\Delta A''(0)+2A'(0)\rho'(0)-\frac{\alpha}{\lambda}A''(0)+\lambda\rho''(0)=0,$$

$$\begin{aligned}D_\rho\Delta\rho''(0)-\frac{2}{\lambda}\left(1-\frac{\alpha}{\lambda}\right)\Delta A''(0)-\nabla\cdot\left[\frac{4}{\lambda}\rho'(0)\nabla A'(0)\right]\\+\nabla\cdot\left[\frac{4}{\lambda^2}\left(1-\frac{\alpha}{\lambda}\right)A'(0)\nabla A'(0)\right]-2A'(0)\rho'(0)-\left(1-\frac{\alpha}{\lambda}\right)A''(0)\\-2\rho'(0)u'(0)-\frac{\lambda\beta}{\lambda-\beta}\rho''(0)-\left(1-\frac{\alpha}{\lambda}\right)u''(0)=0,\end{aligned}$$

and

$$\begin{aligned}D_u\Delta u''(0)-\chi_0\left(\frac{\beta}{\lambda-\alpha}-1\right)\Delta A''(0)-\nabla\cdot\left[2\chi'(0)\left(\frac{\beta}{\lambda-\alpha}-1\right)\nabla A'(0)\right]\\-\nabla\cdot\left[2\chi_0\frac{1}{\lambda}u'(0)\nabla A'(0)\right]+\nabla\cdot\left[2\chi_0\frac{1}{\lambda}\left(\frac{\beta}{\lambda-\alpha}-1\right)A'(0)\nabla A'(0)\right]=0.\end{aligned}$$

Multiply the above three equations by ϕ and integrate, and we should get the following

$$H\left(\int_\Omega\phi A''(0),\int_\Omega\phi\rho''(0),\int_\Omega\phi u''(0)\right)^T+\widehat{h}=0,\tag{3.0.4}$$

https://doi.org/10.1017/S0956792526100357 Published online by Cambridge University Press

where $\widehat{h}$ is the vector containing the lower derivative terms

$$\widehat{h}=\begin{bmatrix} \int_\Omega 2A'(0)\,\rho'(0)\,\phi \\ \left\{\int_\Omega \left(-\nabla\cdot\left[\frac{4}{\lambda}\rho'(0)\,\nabla A'(0)\right]+\nabla\cdot\left[\frac{4}{\lambda^2}\left(1-\frac{\alpha}{\lambda}\right)A'(0)\,\nabla A'(0)\right]\right.\right. \\ \left.\left.-2A'(0)\,\rho'(0)-2\rho'(0)\,u'(0)\right)\phi\right\} \\ \left\{\int_\Omega \left(-\nabla\cdot\left[2\chi'(0)\left(\frac{\beta}{\lambda-\alpha}-1\right)\nabla A'(0)\right]-\nabla\cdot\left[2\chi_0\frac{1}{\lambda}u'(0)\,\nabla A'(0)\right]\right.\right. \\ \left.\left.+\nabla\cdot\left[2\chi_0\frac{1}{\lambda}\left(\frac{\beta}{\lambda-\alpha}-1\right)A'(0)\,\nabla A'(0)\right]\right)\phi\right\} \end{bmatrix}.$$

We know that χ_0 makes H singular. The left eigenvector of H corresponding to 0 is

$$\widehat{\mathbf{P}(\mathbf{x})}=\left(-\frac{D_u\mu(\beta\lambda+D_\rho\mu(\lambda-\alpha))}{(\lambda-\alpha)^2},-\frac{D_u\lambda\mu}{\lambda-\alpha},1\right)^T.$$

We multiply (3.0.4) by $\widehat{\mathbf{P}(\mathbf{x})}$ from the left

$$\widehat{\mathbf{P}(\mathbf{x})}^T H\left(\int_\Omega \phi A''(0),\int_\Omega \phi\rho''(0),\int_\Omega \phi u''(0)\right)^T+\widehat{\mathbf{P}(\mathbf{x})}^T\widehat{h}=\widehat{\mathbf{P}(\mathbf{x})}^T 0 \implies \widehat{\mathbf{P}(\mathbf{x})}^T\widehat{h}=0.$$

We expand $\widehat{\mathbf{P}(\mathbf{x})}^T\widehat{h}$ and use fact that $(A'(0),\rho'(0),u'(0))=\mathbf{P}(\mathbf{x})$. In addition, integration by parts and Green's first identity let us deal with gradients in the following way

$$\int_\Omega \phi(\nabla\phi\cdot\nabla\phi)=\frac{1}{2}\int_\Omega \nabla\phi\cdot\nabla(\phi^2)=-\frac{1}{2}\int_\Omega \phi^2\Delta\phi=\frac{\mu}{2}\int_\Omega \phi^3.$$

We collect terms containing $\chi'(0)$ on the left-hand side (where we also use $\int_\Omega \phi^2=1$) and those containing $\int_\Omega \phi^3$ on the right-hand side

$$2D_u\lambda^2(\lambda-\alpha)(\alpha+\beta-\lambda)\chi'(0)=(C_1\beta+C_2)\int_\Omega \phi^3,$$

where

$$C_1:=-\lambda\,(\chi_0-D_u)\,(-\alpha\chi_0+2D_AD_u\lambda\mu+2D_u\alpha+\lambda\chi_0)\,, \tag{3.0.5}$$

and

$$\begin{aligned} C_2=&-(\lambda-\alpha)\left\{\lambda\left[-2D_u^2\mu\left(D_A(\mu D_\rho-\lambda+\mu)-1\right)+D_u\lambda\chi_0(1-2\mu D_A)-\lambda\chi_0^2\right]\right. \\ &\left.+\alpha\left[2D_u^2\left(\lambda-\mu(D_\rho+2)\right)-3D_u\lambda\chi_0+\lambda\chi_0^2\right]\right\}. \end{aligned} \tag{3.0.6}$$

The coefficients on the left-hand side are non-zero by assumption on the parameters. Hence, $\chi'(0)\neq 0$ if $\beta\neq -C_2/C_1$ and $\int_\Omega \phi^3\neq 0$. This completes part (a).

Remark 3.1. Note that χ_0 depends on β through its definition. Thus, determining β^* such that $C_2\beta^*+C_1\neq 0$ and ensuring that β is independent of χ_0 reduces to solving a quadratic equation. The explicit expression for β^* can be obtained from the discriminant; however, it is algebraically cumbersome and therefore omitted here. Moreover, since $\beta>\lambda-\alpha>0$, one can derive sufficient conditions to guarantee either $-C_2/C_1<\lambda-\alpha$ or $-C_2/C_1<0$.

Remark 3.2. As noted in [8], on a disc domain, a transcritical bifurcation arises because the eigenfunctions of the Laplace operator involve Bessel functions, which lack the symmetry required to ensure $\int_\Omega \phi^3=0$. Consequently, the analysis developed here remains valid in this setting. In contrast, for rectangular domains, the solutions of the Helmholtz equation are products of cosine functions, which satisfy $\int_\Omega \phi^3=0$ (for example, $\int_{[0,\pi]\times[0,\pi]}\cos^3(nx)\cos^3(my)dxdy=0$). Therefore, the same bifurcation scenario

https://doi.org/10.1017/S0956792526100357 Published online by Cambridge University Press

does not directly apply in rectangular domains. This observation is consistent with previous studies by [46, 62], which demonstrate that pitchfork bifurcations are expected in rectangles, where $\chi'(0) = 0$. To analyse the stability of these bifurcating branches, one must therefore examine higher-order terms, in particular $\chi''(0)$.

We follow [8] to verify part (b): we show that $\sigma(0) = 0$ is the eigenvalue of $D\mathcal{F}_{(A,\rho,u)}(\chi, A, \rho, u)$ at $(\chi_0, \mathbf{0})$ with the largest real part. The corresponding eigenvalue problem is

$$\begin{cases} D_A \Delta v_1 - \dfrac{\alpha}{\lambda} v_1 + \lambda v_2 = \sigma v_1, & \text{in } \Omega, \\ D_\rho \Delta v_2 - \dfrac{2}{\lambda}\left(1 - \dfrac{\alpha}{\lambda}\right)\Delta v_1 - \left(1 - \dfrac{\alpha}{\lambda}\right) v_1 - \dfrac{\lambda\beta}{\lambda - \alpha} v_2 - \left(1 - \dfrac{\alpha}{\lambda}\right) v_3 = \sigma v_2, & \text{in } \Omega, \\ D_u \Delta v_3 - \chi\left(\dfrac{\beta}{\lambda - \alpha} - 1\right)\Delta v_1 = \sigma v_3, & \text{in } \Omega, \\ \dfrac{\partial v_1}{\partial \mathbf{n}} = \dfrac{\partial v_2}{\partial \mathbf{n}} = \dfrac{\partial v_3}{\partial \mathbf{n}} = 0, & \text{on } \partial\Omega, \end{cases}$$

which can be rewritten as follows for 3×3 matrices P, Q

$$P\Delta\vec{v} + Q\vec{v} = \sigma\vec{v}. \tag{3.0.7}$$

By spectral theorem, $\vec{v} = \sum_{i=1}^{\infty} \vec{v}_i \phi_i$, where ϕ_i is orthonormal eigenfunction of $-\Delta$ with homogeneous Neumann boundary conditions. If σ is an eigenvalue, then for some i, $\vec{v}_i \neq 0$. Integrate (3.0.7) by ϕ_i, then we should get

$$-P\mu_i\vec{v}_i + Q\vec{v}_i = \sigma v_i.$$

Hence, σ can be represented as an eigenvalue of $-P\mu_i + Q$ for some eigenvalue μ_i of $-\Delta$. On the other hand, any μ_i leads to 3 eigenvalues of (3.0.7) corresponding to the eigenvalues of $-P\mu_i + Q$. To avoid confusion, we denote the eigenvalue of $-\Delta$ that appears in Theorems 2.2, 3.1 as μ_*. We drop the i subscript, then at the bifurcation point, $-P\mu + Q = H$ with $\chi = \chi_0$. We analyse the eigenvalues from the following equation

$$H\left(\int_\Omega v_1\phi, \int_\Omega v_2\phi, \int_\Omega v_3\phi\right)^T = \sigma\left(\int_\Omega v_1\phi, \int_\Omega v_2\phi, \int_\Omega v_3\phi\right)^T.$$

According to Routh–Hurwitz stability criterion, (3.0.1) has roots with non-positive real parts if $a_2 \geq 0$, $a_0 \geq 0$ and $a_2 a_1 \geq a_0$. Our goal is to determine conditions that ensure none of the eigenvalues of $-\Delta$ violate these inequalities. Each coefficient a_i is treated as a polynomial in μ, and the corresponding equalities must be analysed carefully. Note that $a_2 \geq 0$ for all non-negative values of μ.

We focus on $a_0 = 0$, which is a critical point for the condition $a_0 \geq 0$. We already know that, when condition $a_0(\mu, \chi) = 0$ holds first at $\mu = \mu_1^{\text{Neumann}}$, the first Neumann mode bifurcates; when it hits at μ_k^{Neumann}, mode k bifurcates, leading to k-peak steady state patterns. At the bifurcation point $(\chi_0, \mathbf{0})$ with $\mu = \mu_*$, one of the roots of (3.0.1) is $\sigma = 0$, a_0 must be 0, thus considering $a_0 > 0$ is not needed. We get that the other two roots (besides μ_*) are

$$\mu_\circ = 0, \quad \mu_\dagger = \frac{1}{D_A D_\rho}\left[2\left(1 - \frac{\alpha}{\lambda}\right) - \frac{\alpha D_\rho}{\lambda} - \frac{D_A\beta\lambda}{\lambda - \alpha}\right] - \mu_*,$$

where the second one is obtained via Vieta's formula. We need to assume that there are no other eigenvalues of $-\Delta$ in the interval $[\max\{\mu_\circ, \mu_\dagger\}, \max\{\mu_*, \mu_\dagger\}]$ besides $\mu_\circ$, μ_* and $\mu_\dagger$.

We need to guarantee that for μ_*, $\mu_\circ$ and $\mu_\dagger$ (in the case it is non-negative and an eigenvalue of $-\Delta$), the other two roots of (3.0.1) have a negative real part. We do so by looking at $a_2 a_1 - a_0$, whose equation is given by (3.0.3). The coefficients in front of μ^0 and μ^3 are positive, hence by Descartes' rule of signs, we expect at least one negative solution, let it be μ_3. The other two roots can be both positive, negative or complex conjugates. If they are negative or complex, then for any $\mu \geq 0$, the above

https://doi.org/10.1017/S0956792526100357 Published online by Cambridge University Press

polynomial will be positive. If the roots are positive, say $\mu_1 < \mu_2$, we need to put extra conditions that there are no eigenvalues of $-\Delta$ in (μ_1, μ_2). This guarantees that there is no μ for which an associated σ has a positive real part, including $\mu_\circ$, μ_* and $\mu_\dagger$. This concludes part (b). □

Corollary 3.1. *Suppose that μ is the eigenvalue of $-\Delta$ appearing in Theorem 2.2 with normalized eigenfunction ϕ. Suppose that the hypotheses of Theorem 2.2 are satisfied. Assume that $\int_\Omega \phi^3 \neq 0$ and $\beta \neq -C_2/C_1$, where C_1 and C_2 are given by (3.0.5) and (3.0.6)*

Further suppose that

$$-2\left(1-\frac{\alpha}{\lambda}\right)+\frac{D_\rho\alpha}{\lambda}+\frac{D_A\beta\lambda}{\lambda-\alpha}>0.$$

If μ is the first positive eigenvalue of $-\Delta$, then the branch $(\chi(s), A(s), \rho(s), u(s))$ of solution of (EQ) bifurcating from $(\chi_0, \bar{A}, \bar{\rho}, \bar{u})$ is stable for sufficiently small and non-zero $|s|$.

Proof. With the same notation as in the proof of Theorem 3.1, suppose that

$$-2\left(1-\frac{\alpha}{\lambda}\right)+\frac{D_\rho\alpha}{\lambda}+\frac{D_A\beta\lambda}{\lambda-\alpha}\geq 0.$$

In this case, the coefficients of μ^1 and μ^2 in (3.0.3) are positive, which implies that no positive roots exist. However, this condition also forces $\mu_\dagger$ to be negative. Consequently, stability requires μ_* to be the first eigenvalue of $-\Delta$, since we must ensure that no eigenvalues lie in the interval $(0, \mu_*)$. □

With Corollary 3.1, we arrive at a dichotomy. If

$$-2\left(1-\frac{\alpha}{\lambda}\right)+\frac{D_\rho\alpha}{\lambda}+\frac{D_A\beta\lambda}{\lambda-\alpha}>0, \tag{3.0.8}$$

then stability is guaranteed only when μ corresponds to the first positive eigenvalue. On the other hand, if

$$-2\left(1-\frac{\alpha}{\lambda}\right)+\frac{D_\rho\alpha}{\lambda}+\frac{D_A\beta\lambda}{\lambda-\alpha}<-\mu D_A D_\rho<0, \tag{3.0.9}$$

then $\mu_\dagger > 0$, and stability requires that no eigenvalues of Δ fall within the interval $(\min\{\mu,\mu_\dagger\}$, $\max\{\mu,\mu_\dagger\})$ (recall, $\mu = \mu^*$). This condition is less restrictive on μ_*, since it does not force it to be the first eigenvalue. However, in this case, one must further ensure that no eigenvalues are present between r_1 and r_2, the positive solutions of (3.0.3), if such exist.

These inequalities, and the resulting stability regions, depend sensitively on parameter choices. For instance, if $D_\rho > 2\frac{\lambda-\alpha}{\alpha}$, then (3.0.8) holds, while if $D_\rho < 2\frac{\lambda-\alpha}{\alpha}$ and $D_A < \frac{(-D_\rho\alpha+2(\lambda-\alpha))(\lambda-\alpha)}{\lambda(\beta+D_\rho\mu(\lambda-\alpha))}$, then (3.0.9) applies. Mathematically, this shows that smaller diffusion rates broaden the range of eigenvalues that can support stable non-constant branches, i.e. patterned steady states.

The stability of the uniform steady state depends very sensitively on the diffusion parameters of the model. Mathematically, the key inequalities show that when offender diffusion (D_ρ) and attractiveness diffusion (D_A) are relatively large, the system tends to remain close to uniform, and only the simplest spatial modes can be stable. By contrast, when both diffusion rates are small, the conditions for stability relax, and more spatial modes are permitted. In this regime, the uniform steady state can lose stability, and the system may bifurcate to non-uniform solutions – steady patterns that represent spatial clustering.

From a criminological perspective, these bifurcation points can be interpreted as thresholds in offender and guardian mobility. When offenders move broadly and randomly across space and when the attractiveness of a crime event spreads widely, local concentrations of crime are smoothed out. However, if offender movement is limited and the attractiveness effect remains strongly localized, the system can cross a threshold where uniform crime distributions are no longer sustainable. Instead, stable heterogeneous patterns emerge, corresponding to persistent hotspots. Social science research suggests that such mechanisms may underlie the persistence of crime in certain neighbourhoods. Limited offender mobility, coupled with strong near-repeat effects, reinforces clustering and creates conditions where particular areas remain chronically affected. In this sense, the mathematics formalizes a well-known observation

https://doi.org/10.1017/S0956792526100357 Published online by Cambridge University Press

in criminology: that reduced movement and strong local feedback can lock specific places into cycles of concentrated criminal activity. While empirical confirmation in the exact setting of this model is still lacking, the analysis provides a plausible theoretical explanation for the formation and persistence of crime hotspots.

4. Hopf bifurcations and time-periodic dynamics

In this section, we investigate Hopf bifurcations, which correspond to the emergence of periodic solutions. Following a similar approach as in the previous section, we demonstrate that, under appropriate conditions, these cycles exist. We further validate the theoretical findings through numerical simulations of the original system. Here, we follow the framework developed in [39], which studies a one-dimensional version of (E). We extend their analysis by treating eigenvalues on general domains, without relying on explicit wavemode vectors.

Note that following Theorem 4.1 is stated for the shift problem (EP), but it holds for the original system (E).

Theorem 4.1. *Let μ be a positive eigenvalue of $-\Delta$ with homogeneous Neumann boundary condition such that $a_1(\mu) > 0$ in (3.0.1), and μ be larger than local maximizer of χ_*, defined as follows*

$$\chi_* := \frac{1}{\beta+\alpha-\lambda}\left\{\frac{a_1 a_2}{D_u\mu} - (\lambda-\alpha) - \frac{\alpha\beta}{\lambda-\alpha} - \mu\left[-2\left(1-\frac{\alpha}{\lambda}\right) + \frac{D_\rho\alpha}{\lambda} + \frac{D_A\beta\lambda}{\lambda-\alpha}\right] - \mu^2 D_A D_\rho\right\}. \tag{4.0.1}$$

Then system (EP) has in a neighbourhood of $(\chi_*, \mathbf{0}) \in V$ a unique one-parameter family $\gamma(s); 0 < s < \varepsilon$ of noncritical periodic orbits. More precisely: there exists $\varepsilon > 0$ and

$$(\chi(\cdot), A(\cdot), \rho(\cdot), u(\cdot), T(\cdot)) \in C^\infty((-\varepsilon, \varepsilon), V \times \mathbb{R}^+)$$

with

$$(\chi(0), A(0), \rho(0), u(0), T(0)) = \left(\chi_*, \bar{A}, \bar{\rho}, \bar{u}, \frac{2\pi}{\sqrt{a_1(\mu)}}\right)$$

such that

$$\gamma(s) := \gamma(A(s), \rho(s), u(s)), \quad 0 < s < |\varepsilon|$$

is a noncritical periodic orbit of (EP) with $\chi = \chi(s)$ of period $T(s)$ passing through $A(s), \rho(s), u(s) \in Y$. Moreover, the family $\{\gamma(s); 0 < s < \varepsilon\}$ contains every noncritical periodic orbit of (EP) lying in a suitable neighbourhood of $(\chi_*, \mathbf{0}, T(0)) \in V \times \mathbb{R}^+$, and $\gamma(s_1) \neq \gamma(s_2)$ for $s_1 \neq s_2$.

Proof. We verify that the conditions of Theorem 1 in [1] are satisfied. In addition, we follow the proof strategies developed in [39, 56]. Specifically, we analyse the eigenvalues of (2.1.2), the linearization of $\mathcal{F}$ at $\mathbf{0}$. The procedure mirrors our earlier approach: multiply by ϕ and integrate over the domain. This again reduces the problem to studying the characteristic equation of H, defined in (3.0.1) and (3.0.2), and determining the conditions under which purely imaginary roots arise.

Let σ_2 and σ_3 be purely imaginary roots of the form $\pm i\omega_0$ with $\omega_0 > 0$, and let σ_1 denote the remaining real root. Then, (3.0.1) can be rewritten as

$$(\sigma - \sigma_1)(\sigma^2 + \omega_0^2) = \sigma^3 - \sigma_1\sigma^2 + \omega_0^2\sigma - \sigma_1\omega_0^2.$$

It follows that $\sigma_1 = -a_2(\mu) < 0$ and $\sigma_{2,3} = \pm i\sqrt{a_1(\mu)}$. To guarantee that the roots are purely imaginary, we require $a_1(\mu) > 0$, which holds whenever μ is chosen outside the real roots of $a_1(\mu)$. The critical bifurcation value $\chi_*(\mu)$ is then defined by the condition $a_2(\mu)a_1(\mu) = a_0(\mu)$. In general, the rational function of μ given in (4.0.1) is continuous but not necessarily injective. Let μ_M denote a real local maximizer of this function. Then, for any $\chi_*(\mu) > \chi_*(\mu_M)$, the corresponding value of μ is uniquely determined.

https://doi.org/10.1017/S0956792526100357 Published online by Cambridge University Press

Finally, we need to check the transversality condition. Let $\sigma_1(\chi)$ and $\sigma_{2,3}(\chi) = p(\chi) + iq(\chi)$ be solutions to (3.0.1) in the neighbourhood of $\chi = \chi_*$. Then, upon substitution and equating the coefficient in front of the power of σ, we get

$$\begin{cases} -a_2 = 2p(\chi) + \sigma_1(\chi), \\ a_1 = p^2(\chi) + q^2(\chi) + 2p(\chi)\sigma_1(\chi), \\ -a_0 = (p^2(\chi) + q^2(\chi))\sigma_1(\chi). \end{cases}$$

Differentiating with respect to χ, we get that $a_0(\mu)' = D_u\mu(\lambda - \alpha)\left(\frac{\beta}{\lambda-\alpha} - 1\right) > 0$.

$$\begin{cases} 0 = 2p'(\chi) + \sigma_1'(\chi), \\ 0 = 2p(\chi)p'(\chi) + 2q(\chi)q'(\chi) + 2p'(\chi)\sigma_1(\chi) + 2p(\chi)\sigma_1'(\chi), \\ a_0' = 2(p(\chi)p'(\chi) + q(\chi)q'(\chi))\sigma_1(\chi) + (p^2(\chi) + q^2(\chi))\sigma_1'(\chi). \end{cases}$$

We evaluate at $\chi = \chi_*$, where $p(\chi_*) = 0$, $q(\chi_*) = \sqrt{a_1(\mu)}$ and $\sigma_1(\chi_*) = -a_2(\mu)$. Thus,

$$\begin{cases} 0 = 2p'(\chi_*) + \sigma_1'(\chi_*), \\ 0 = 2\sqrt{a_1}\, q'(\chi_*) - 2p'(\chi_*)a_2, \\ a_0' = -2\sqrt{a_1}\, q'(\chi_*)a_2 + a_1\sigma_1'(\chi_*). \end{cases}$$

Solving this system for $(p'(\chi_*),\ q'(\chi_*),\ \sigma_1'(\chi_*))^T$, we obtain

$$p'(\chi_*) = -\frac{2a_0'}{a_1(\mu) + a_2^2(\mu)} < 0,$$

where the inequality follows from the assumption that μ lies outside the interval where $a_1(\mu) < 0$. □

Remark 4.1. The main difference between our proof and that in [39] is that our assumptions are based on the eigenvalues of $-\Delta$, rather than on the wave mode vector $\vec{k}$, which reduces to a scalar in one dimension. One could also verify the stability of the resulting periodic solutions following the same methodology as in that paper. Since the procedure does not directly depend on the spatial dimension, we expect analogous conclusions when χ is treated as a function of μ, and therefore the corresponding proof is omitted. The primary purpose of this section is to show how the eigenvalues of the negative Laplacian can be used to decouple the effects of domain geometry and spatial dimension from the analysis of the model's reaction dynamics, using Hopf bifurcation as an illustrative example. While the eigenvalues themselves depend on the spatial dimension and the geometry of the domain, this framework allows the bifurcation analysis to be carried out in a way that is independent of these geometric details, which enter only through the spectral parameter.

Remark 4.2. One may notice that the analysis performed and hence the results of Sections 2, 3 and 4 are related to the parameter $0 < s \ll 1$, which is a proxy of how close we are to a constant steady state. There is an alternative approach to establishing stability and bifurcation results, prominently presented in [54]. The authors consider a singular perturbation analysis and a nonlocal eigenvalue problem for $D_A \sim \mathcal{O}(\epsilon^2)$ and $D_\rho \sim D_0/\epsilon^2$, where $D_0 \sim \mathcal{O}(1)$. While primarily interested in investigating the emergence of local concentrations of high values of scalar fields, they have established extensive results on stability and bifurcations (including Hopf ones) for a wide range of parameters far from the equilibrium. Besides the overall methodology and the relative distance from spatial homogeneity, we note a few differences between this paper and [54]. First, the systems are slightly different: in ρ equation of system (E), the removal rate of criminals by the police is $-u$ in [54], rather than $-\rho u$. This affects the expression for constant steady-state solutions and the subsequent linear stability analysis. Second, similar to [39], the authors in [54] considered only a one-dimensional case; hence, the previous remark holds as well. Third,

https://doi.org/10.1017/S0956792526100357 Published online by Cambridge University Press

the parameters in our work are not restricted (directly); instead, we impose conditions on the negative Laplacian eigenvalues. Hence, our results may be viewed as more general, yet more obscure than those in [54]. There are additional differences to mention; however, in the end, both papers complement each other in providing a more complete picture of how bifurcation analysis can be performed in RAD systems such as (E).

The bifurcation value χ_* determines the onset of Hopf instabilities, where the spatially homogeneous steady states lose stability and give rise to oscillatory behaviour. These periodic solutions exhibit spatio-temporal behaviour in that they repeat not only in time but also exhibit structured, recurring patterns in space. This behaviour will be observed in the numerical simulations illustrated in Figure 2c, for example. In social-science terms, this suggests that when policing intensity crosses these thresholds, crime dynamics may enter into recurring cycles – periods of high and low crime concentrated in particular neighbourhoods – rather than settling into a stable equilibrium. Such cyclical hotspot activity has been observed empirically and reflects the limitations of static policing strategies.

5. Numerical simulations and pattern formation

In this section, we numerically investigate heterogeneous steady states in two dimensions, a natural setting for studying urban crime since it reflects how hotspots emerge and persist across neighborhoods. Previous studies [39, 62] employed linear stability analysis to identify key thresholds, denoted by χ^- and χ^+ (see [62] for precise definitions). The constant steady state is linearly stable whenever $\chi^- < \chi < \chi^+$. Crossing these thresholds corresponds to intensities at which uniform crime–guardian equilibria destabilize, producing either stationary clustering (steady-state bifurcation) or cycling hotspots (Hopf). From a social perspective, these bifurcation values mark thresholds of police responsiveness: when policing intensity remains between χ^- and χ^+, uniform safety can be maintained, but crossing either boundary destabilizes the system, potentially leading to persistent or oscillatory crime concentrations.

Here, we focus on cases in which at most one of these inequalities is violated. For reproducibility and further exploration, the simulation codes are publicly available: parameter exploration can be carried out with https://github.com/MaYeatCo/urban_bifurcation, while individual one- and two-dimensional simulations can be found in https://github.com/MaYeatCo/urban_suppression.

Since the number of parameters is large, we fix most of them and focus on how the diffusion rates affect the solutions. Specifically, we consider the case of hotspot policing, where police movement mimics that of crime agents, *i.e.*, $\chi = 2$ and $D_u = D_\rho$, (in later subsections, we will consider the case of various D_ρ vs D_u and D_u vs χ, so these assumptions are not true throughout the whole numerical simulations). Our simulations are conducted in two dimensions on a square domain with side length L. We perform a parameter sweep over a fixed range of D_A and D_ρ and compute the orderings of χ, χ^-, and χ^+. The results are summarized in Figure 1. To create this figure, we apply the linear stability results from [39, 62] using wave numbers/vectors k. We then verify that the stability conditions hold across a wide range of $|k|$. All possible orderings are represented by regions I–VI, and these regions correspond to different policing thresholds, where small changes in deployment intensity can qualitatively alter crime distributions. For instance, the border between regions I and III occurs precisely when $a_2(\mu)a_1(\mu) = a_0(\mu)$ in Theorem 4.1 (or equivalently $a_2(k)a_1(k) = a_0(k)$ in Proposition 2.1 in [39]). Our objective is to determine whether periodic or near-periodic solutions emerge, thereby confirming the theoretical predictions. After identifying the stability regions, we carry out numerical simulations.

We select three parameter combinations within the interior of the regions (labelled A–C), as well as three parameter combinations located around the borders between region I and the others (labelled D–F). Here, we did not conduct simulations for regions IV–VI in Figure 1. These regions lie farther from region I and correspond to cases where multiple Routh–Hurwitz conditions are violated, making the system's behaviour less predictable. As shown in [39], solutions in these regimes can exhibit chaotic

https://doi.org/10.1017/S0956792526100357 Published online by Cambridge University Press

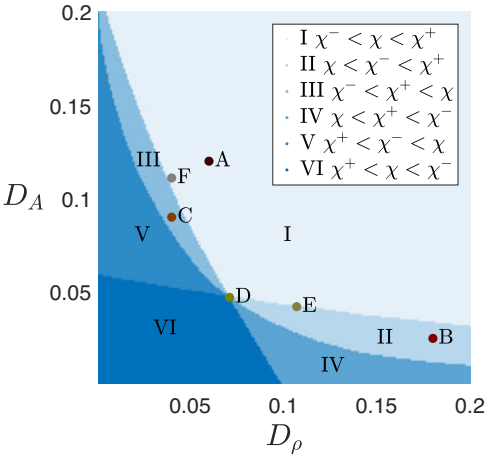


Figure 1. *Illustration of the effect of diffusion rates on the ordering of χ, χ^- and χ^+ obtained from linear stability analysis. Roman numerals indicate the corresponding inequality regimes, while letters denote parameter combinations selected for further simulations. Region I corresponds to the linearly stable regime. The remaining parameters are fixed at $\alpha = 1.0, \beta = 1.0, \lambda = 1.5, \chi = 2, L = \pi$. Each region represents a distinct ordering of χ, χ^- and χ^+. Note that this figure illustrates only the predictions from linear stability analysis. Non-linear effects may significantly influence the solution behaviour, particularly near the boundaries between regions.*

dynamics. Examples of such less predictable behaviour (in the theoretical sense) will be presented in the following subsections.

We use the PDE toolbox in MATLAB [51, 52] to perform numerical simulations. As simulations are done in two dimensions, it is not straightforward to depict the evolution of the solution. Thus, we choose to track changes in overall amplitude via a root mean square function. All solutions are initiated at the steady-state constant plus a small perturbation (0.01) using a cosine function. The time evolutions are shown in Figure 2. We use the root mean square metric, defined as $\mathrm{RMS}[f(x,t)] = \sqrt{|\Omega|^{-1} \int_\Omega f(\mathbf{x},t)^2 d\mathbf{x}}$. In addition, we plot the final frames of the simulation to show the patterns they exhibit, see Figure 3.

We now turn to Figures 2 and 3 for a more detailed examination of the dynamics. At point A, corresponding to region I, perturbations decay monotonically, and the solution converges to the spatially uniform steady state, in full agreement with the linear stability predictions. At points B, D, and E, the solution amplitude increases and then saturates at a nonzero level, yielding spatially heterogeneous but temporally stationary states. These patterns may appear as hotspots, symmetric arrangements or related structures. At point C, located in region III, the long-time dynamics approach a time-periodic orbit. Near regime boundaries, as exemplified by point F, the system exhibits more intricate dynamics, with oscillations of varying amplitude that indicate the onset of mixed-type or higher-order bifurcations. Such transitional regimes call for more refined analysis, either through extended simulations or by applying weakly non-linear techniques. In summary, the numerical results confirm the existence of periodic solutions, consistent with the statement of Theorem 4.1.

5.1. Time-periodic patterns

In two-dimensional simulations, the solution may require a considerable time to converge, as can be observed in Figure 2f. To investigate periodic behaviour more efficiently, we therefore turn to a one-dimensional setting, where simulations are computationally less demanding. This reduction not only

https://doi.org/10.1017/S0956792526100357 Published online by Cambridge University Press

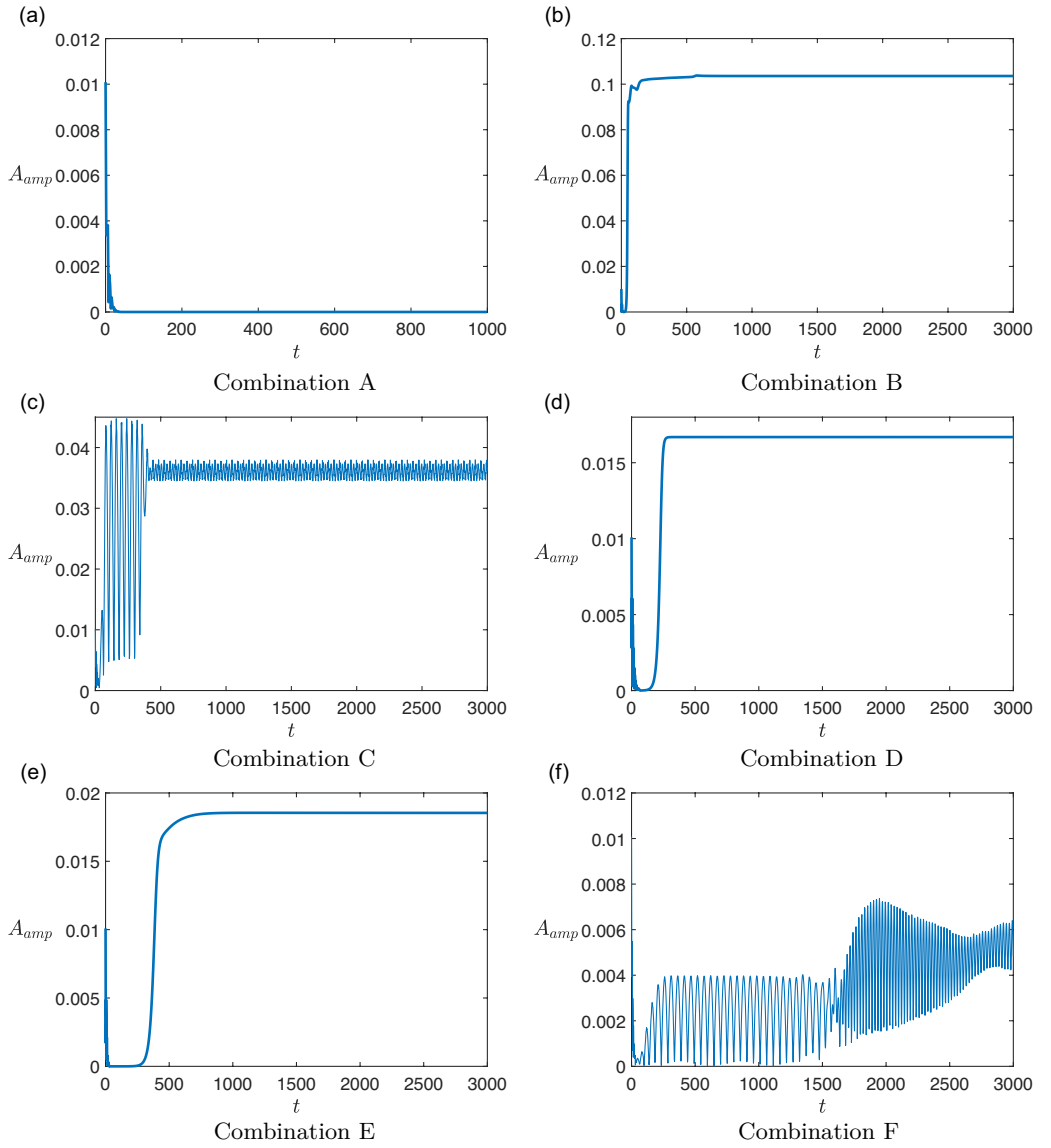


Figure 2. *Examples of amplitude evolutions from Figure 1, computed using* $A_{amp} = \mathrm{RMS}[A(\mathbf{x}, t) - \lambda]$*, illustrate how diffusion rates shape system dynamics. In* ***(a)****, amplitudes decay monotonically, confirming the stability of the uniform steady state. In* ***(b)****, they saturate at a non-zero level, producing stationary hotspots. In* ***(c)****, periodic oscillations arise through a Hopf bifurcation, resembling recurrent "crime waves." in* ***(d)****, irregular oscillations signal mixed or higher-order bifurcations and parameter sensitivity. Near regime borders, as in* ***(e)*** *and* ***(f)****, small perturbations can trigger clustering or quasi-periodic oscillations with irregular amplitudes, marking transitions to more complex or weakly chaotic behaviour. Together, these results show how the system shifts from uniform stability to persistent hotspots, oscillatory patterns and chaotic regimes as diffusion rates vary.*

https://doi.org/10.1017/S0956792526100357 Published online by Cambridge University Press

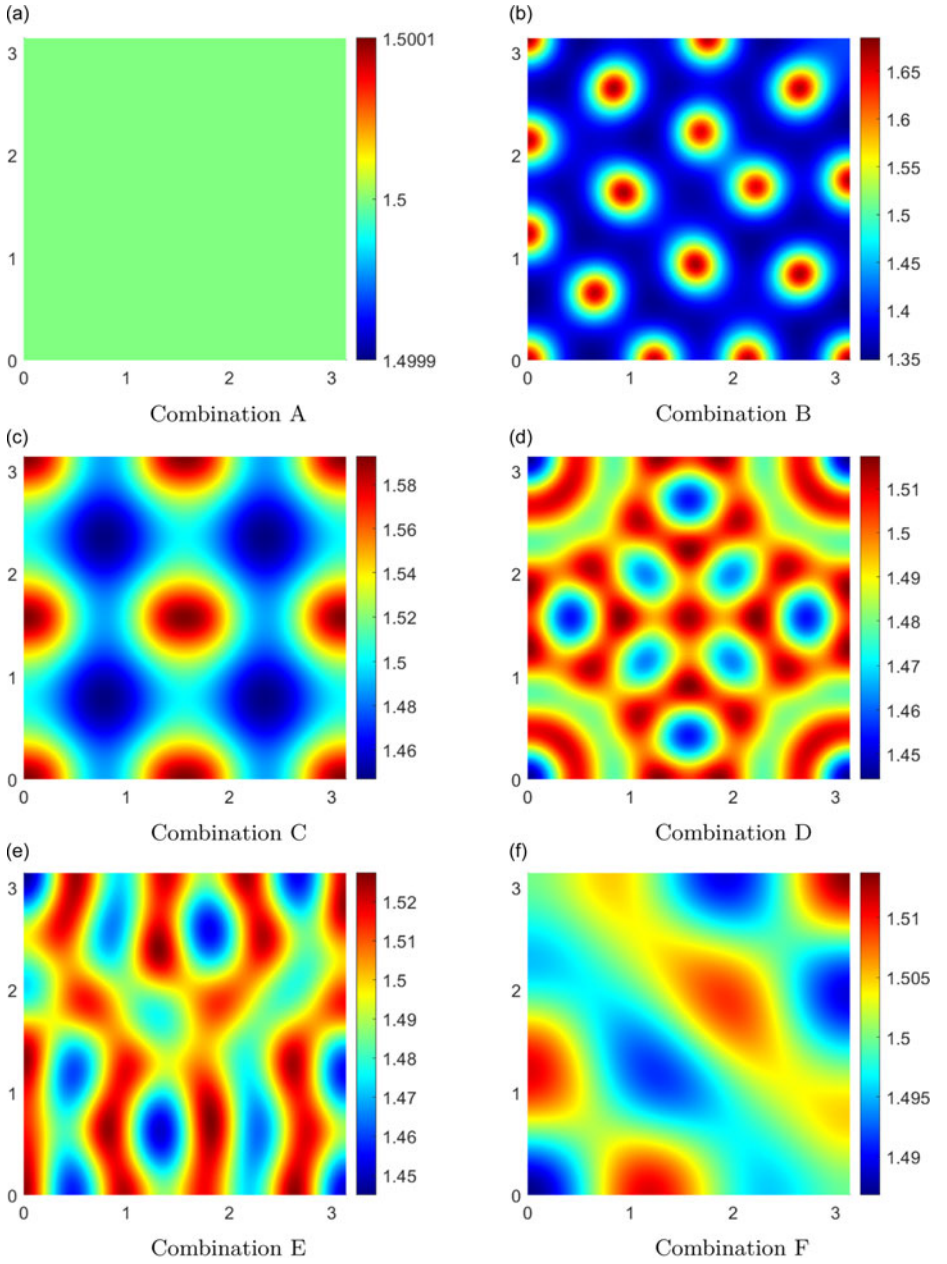
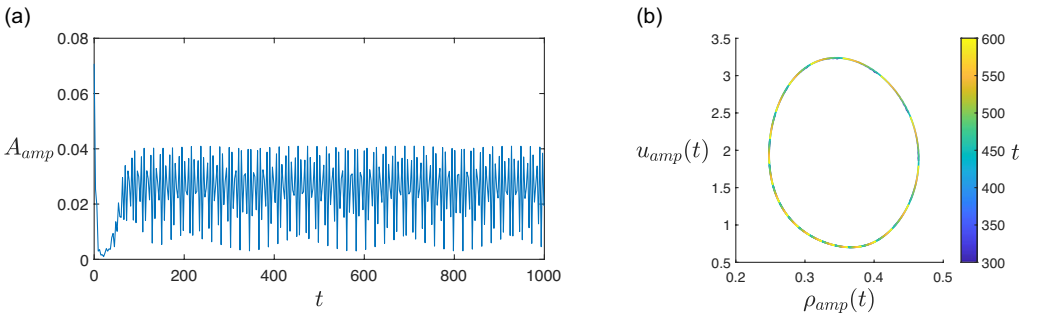


Figure 3. *Examples of patterns corresponding to the points in Figure 1. The diffusion rates are* ***(a)*** *region I,* $D_A = 0.12, D_\rho = 0.06$*;* ***(b)*** *region II,* $D_A = 0.025, D_\rho = 0.18$*;* ***(c)*** *region III,* $D_A = 0.09, D_\rho = 0.04$*;* ***(d)*** *Intersection of all regions,* $D_A = 0.047, D_\rho = 0.071$*;* ***(e)*** *near the border between regions I and II,* $D_A = 0.042, D_\rho = 0.107$*;* ***(f)*** *near the border between regions I and III,* $D_A = 0.111, D_\rho = 0.04$*. The remaining parameters are fixed at* $\alpha = 0.5, \beta = 1.0, \lambda = 0.75, \chi = 2, L = \pi$*. The snapshots reveal distinct regimes: uniform states* ***(a)****, stationary hotspots* ***(b)****, periodic oscillations* ***(c)****, irregular mixed patterns at parameter intersections* ***(d)*** *and near-threshold behaviour with localized clustering or quasi-periodic fluctuations* ***(e)****,* ***(f)****. Together, they illustrate how tuning diffusion rates drives transitions from uniform stability to heterogeneous clustering, oscillations and complex dynamics.*

https://doi.org/10.1017/S0956792526100357 Published online by Cambridge University Press



Amplitude evolution of A Phase-portrait of amplitudes ρ-u

Figure 4. *Representation of a one-dimensional simulation of (E) with the same parameters as in 2c.* ***(a)*** *Emergence and stabilization of periodic behaviour in the amplitude of the A component, $A_{amp} = \mathrm{RMS}[A(x,t) - \lambda]$. Data are sampled every 3 time units to provide a clearer visualization of the oscillations. The figure shows that, after an initial transient, the solution does not converge to a steady state but instead settles into sustained periodic dynamics, reflecting the onset of a Hopf bifurcation.* ***(b)*** *Limit cycle in the ρ_{amp} versus $u_{amp} = (\mathrm{RMS}[\rho(x,t) - \bar{\rho}]$ versus $\mathrm{RMS}[u(x,t) - \bar{u}])$ phase portrait for $t \in [300, 600]$, with trajectories represented in colour. The closed orbit indicates that the dynamics of the offender density (ρ) and the guardian density (u) are locked into a recurring cycle rather than stabilizing to an equilibrium. These results highlight the transition from stationary to oscillatory crime–policing patterns. In dynamical systems terms, the system crosses a bifurcation threshold where uniform hotspots lose stability and periodic oscillations emerge. From a criminological perspective, this suggests that crime and enforcement densities may fluctuate in sustained cycles – so hotspots not only persist but also oscillate in intensity and location over time, echoing empirical observations of recurring "crime waves.".*

decreases the run-time but also allows the use of a smaller time step Δt, improving the numerical accuracy. While simplified, the one-dimensional results remain informative, as they capture the essential dynamics and can be extended qualitatively to the two-dimensional case, particularly concerning the existence of distinct classes of solution behaviour.

To demonstrate the comparison between the two domains, we simulate system (E) over the interval under the same combination as in Figure 2c. The results are illustrated in Figure 4. Figure 4a is the one-dimensional counterpart of Figure 2c. Although there are differences, the overall qualitative behaviour is the same between the two. Moreover, the simulations over an interval take a shorter time to stabilize (200 in 1-D versus 500 in 2-D), and we see a clearer periodic solution, i.e. we are more confident in characterizing this behaviour as periodic. This trend is further supported in Figure 4b, where we observe a limit cycle. The period seems to be ≈ 240 time units. Further time-series analysis can be performed, which can be helpful when examining multiple simulations, such as a parameter sweep setting in Figure 1, but this is beyond the scope of this paper. Instead, in the following section, we utilize the speed and reliability of one-dimensional simulations to shed light on another type of solution: chaos.

5.2. Exploring chaos

A natural question is what occurs in regions IV–VI of Figure 1. As shown in [39], under certain parameter regimes – for instance, when diffusion rates are sufficiently small – the system can exhibit chaotic behaviour. To provide further evidence of this phenomenon, we present the bifurcation diagram in Figure 5. The diagram reveals that as diffusion decreases, new dynamical behaviours emerge. The first periodic solution appears around $D_\rho = 0.06$. At $D_\rho = 0.03$, successive period-doublings occur, eventually leading to the onset of chaos. We explore these regimes through representative solutions in

https://doi.org/10.1017/S0956792526100357 Published online by Cambridge University Press

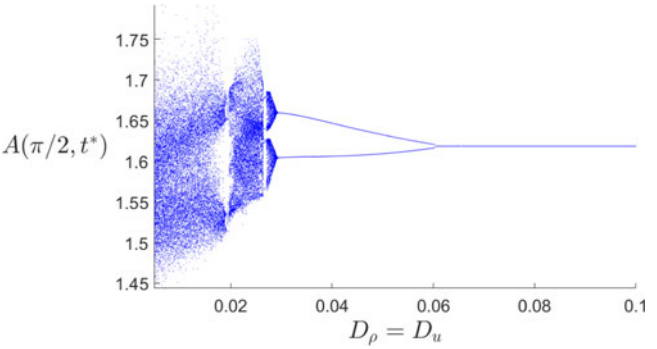


Figure 5. *Bifurcation diagram of the midpoint value $A(\pi/2, t^*)$ in the one-dimensional simulation of (E) in $(0, \pi)$ with initial perturbation of the form $0.05\cos(x)$. The y-axis records all extreme values of $A(\pi/2, t)$ with $t \in [800, 1000]$, after transients have decayed. t^* denotes a maximizer or a minimizer. Simulations are run up to $T_{\max} = 1000$, treating $t \in [0, 800]$ as transient. Parameters are fixed at $D_A = 0.1$, $\alpha = \beta = 1$, $\lambda = (1 + \sqrt{5})/2$ and $\chi = 2$, with varying D_ρ to reveal the bifurcation structure. The diagram illustrates how decreasing D_ρ drives qualitative changes in the long-term behaviour of the system. For relatively large diffusion rates, solutions converge to spatially uniform steady states, consistent with linear stability predictions. As D_ρ decreases, periodic solutions emerge, followed by successive period-doublings, and eventually chaotic dynamics. This transition reflects the loss of stability of homogeneous states and the onset of complex spatio-temporal behaviour. In particular, the appearance of chaos indicates that small diffusion rates can amplify non-linear feedback, leading to unpredictable but persistent fluctuations in the crime–policing system.*

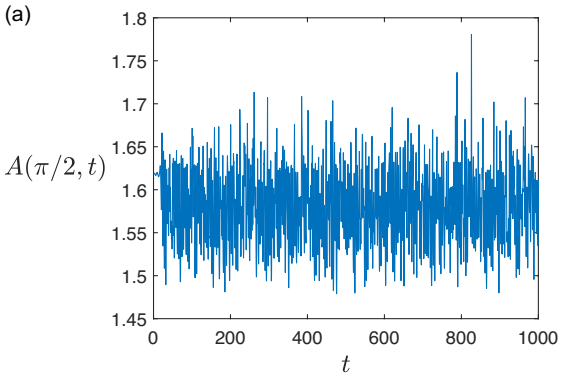
Figures 6 and 7. In Figure 6a, the time series of $A_m(t)$ displays unpredictable fluctuations, and the system quickly settles into this chaotic regime. By contrast, Figure 7a shows a clear periodic orbit, though it takes longer for the dynamics to stabilize, and the oscillation frequency is relatively high ($\gg 1$).

The corresponding phase portraits for ρ and u further illustrate the difference: in the chaotic case (Figure 6b), trajectories approach a strange attractor, whereas in the periodic case (Figure 7b), a well-defined closed orbit is observed. Chaotic solutions also exhibit larger deviations from the steady state. For example, although $\bar{u} = 1$ in both cases, in the periodic regime u oscillates between approximately 0.65 and 1.2, while in the chaotic regime it can range from near zero to as high as nine. Many additional phenomena could be uncovered with a more detailed analysis. However, it is worth noting that the theory of chaos in infinite-dimensional PDE systems is less developed than in finite dimensions, making rigorous characterization challenging. Nevertheless, the present model appears to provide a promising and mathematically rich setting for future research on spatiotemporal chaos in criminology-inspired systems.

5.3. Further exploration of parameter space

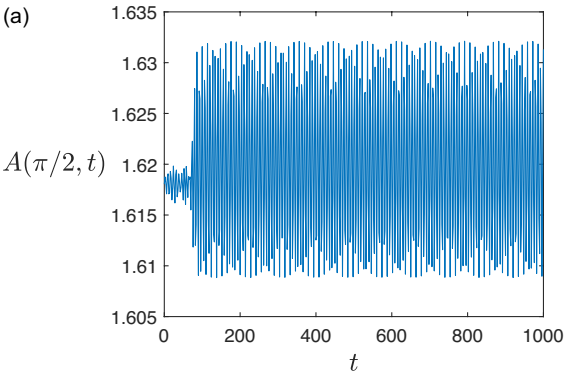
In this section, we complement our theoretical findings by examining how parameter choices affect the behaviour of solutions. Specifically, we focus on the movement dynamics of real agents – namely, how variations in the diffusion and advection rates of ρ and u influence the system. All other parameters are held fixed. In this way, our analysis can be interpreted as studying the outcomes of strategic decisions from one side: given the random movement of criminal agents, what spatial patterns or effects might arise under different police deployment strategies? To address this, we use an interval domain for phase-plane simulations, which enables us to employ sufficiently small time steps to capture the dynamics at lower diffusion values. Recall that large diffusion rates lead to a linearly stable regime, a case that has already been analysed.

https://doi.org/10.1017/S0956792526100357 Published online by Cambridge University Press



Time evolution of the midpoint of A | Phase-portrait of midpoints of $\rho - u$

Figure 6. *Representations of the chaotic solution to (E) with the same parameters as in Figure 5, except that $D_\rho = D_u = 0.01$. As before, we investigate dynamics at the spatial midpoint, $x = \pi/2$.* ***(a)*** *Time evolution of $A(\pi/2, t)$. Instead of converging to a steady state or periodic orbit, the trajectory exhibits irregular oscillations with no discernible repeating pattern, characteristic of chaos.* ***(b)*** *Phase portrait of the non-transient trajectories of $\rho(\pi/2, t)$ and $u(\pi/2, t)$ for $t \in [800, 1000]$, with colours indicating temporal progression (dark blue at $t = 800$, yellow at $t = 1000$). The trajectory does not close into a limit cycle but instead wanders in a complex set consistent with a strange attractor. Together, these figures again illustrate that very small diffusion rates destabilize uniform or periodic states and produce chaotic dynamics. From a criminological perspective, this corresponds to volatile crime–policing interactions, where hotspots neither stabilize nor repeat regularly but instead fluctuate unpredictably over time.*



Time evolution of the midpoint of A_m | Phase-portrait of midpoints $\rho - u$

Figure 7. *Representations of a periodic solution to (E). The parameters are the same as in Figure 5, but additionally $D_\rho = D_u = 0.05$.* ***(a)*** *The full time of evolution of $A(\pi/2, t)$ is given.* ***(b)*** *The non-transient $\rho(\pi/2, t)$ and $u(\pi/2, t)$ are plotted against each other. The colours represent the time: dark blue – $t = 800$ and yellow – $t = 1000$. When compared to Figure 6, we only slightly increased diffusion rates, yet now the trajectory is an orbit after passing the aperiodic transient state. Similarly to Figure 4, we observe "crime waves". Moreover, the overall amplitudes are smaller. This figure, along with 6, demonstrates how changes in the agents' movement affect the solution.*

https://doi.org/10.1017/S0956792526100357 Published online by Cambridge University Press

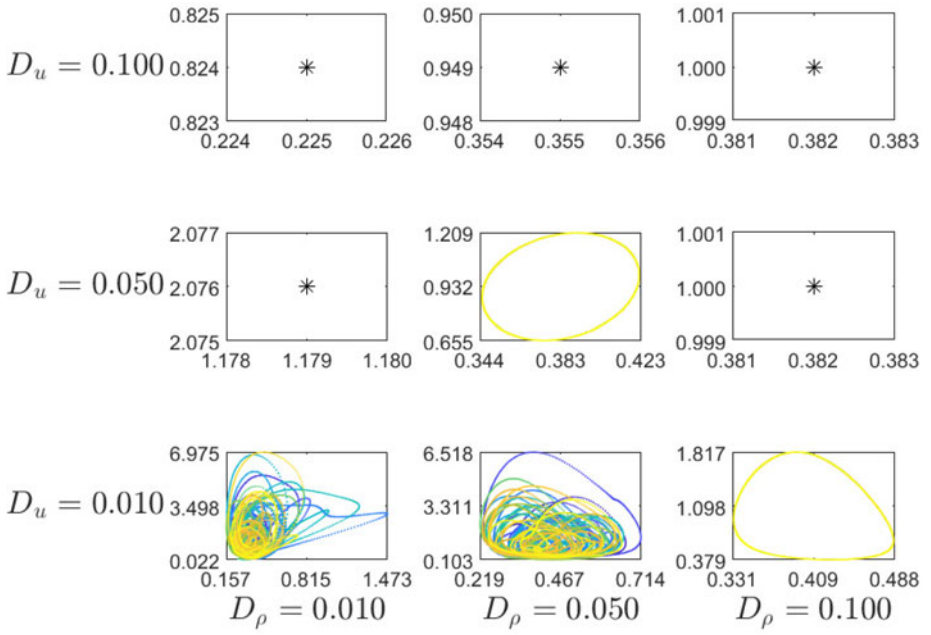


Figure 8. *Solutions to (E) for various D_ρ (columns) and D_u (rows). The non-transient $\rho(\pi/2, t)$ and $u(\pi/2, t)$ are plotted against each other. The remaining parameters are $D_A = 0.1$, $\alpha = \beta = 1$, $\lambda = (1+\sqrt{5})/2$, $\chi = 2$. The colours represent the time: dark blue – $t = 800$ and yellow – $t = 1000$. The star represents the constant-in-time solutions. Whenever $\rho(\pi/2, t) = 0.382$ and $u(\pi/2, t) = 1$, this indicates constant-in-space solutions as well. We observe that the reduction in the diffusion, which is a proxy for random movement here, leads to less predictable behaviour, destabilizing the crime landscape.*

Similar to Figure 1, we examine the influence of diffusion rates, but with D_A held fixed. In particular, we explore combinations of relatively small values of D_ρ and D_u, with the results shown in Figure 8. As expected, smaller diffusion rates lead to chaotic behaviour. As diffusion rates increase, solutions tend to become spatially heterogeneous or exhibit periodic patterns. Only when both diffusion rates are sufficiently large ($D_\rho > 0.1$ and $D_u > 0.05$) does the system converge to constant solutions. This relationship can be interpreted as crime-stabilizing strategies: police agents may increase their diffusion to drive the system towards a constant-in-time state. Moreover, we observe that temporally varying solutions typically attain significantly higher and lower amplitudes compared to the constant steady-state values, with smaller diffusion rates producing larger deviations. This observation suggests a potential crime-suppression strategy: wait until the density of criminal agents reaches a low point and then intervene to stabilize the system at that level (see [62] for additional suppression strategies).

Next, we consider a scenario in which the diffusion rate of crime agents is fixed while the police advection rate is varied. This provides an alternative perspective for exploring potential strategies and policy outcomes. The corresponding results are shown in Figure 9. Recall that $\chi = 2$ represents hotspot policing, where the police advection rate matches that of crime agents (second row). Increasing χ concentrates police more strongly around hotspots (first row), whereas flipping the sign corresponds to off-hotspot policing, where police avoid areas of high attractiveness (last row). We also examine the case with no advection (third row). We observe that increasing χ while keeping D_u small results in chaotic or periodic behaviour, which can be attributed to the fact that $\chi > \chi^+$. By contrast, increasing D_u appears to stabilize the system, at least in a temporal sense.

However, as shown by the linear stability analysis in [62], no value of D_u with fixed $\chi = 4$ can shift the system into the linearly stable regime; in other words, there does not exist $D_u > 0$ such that $\chi^- < \chi < \chi^+$

https://doi.org/10.1017/S0956792526100357 Published online by Cambridge University Press

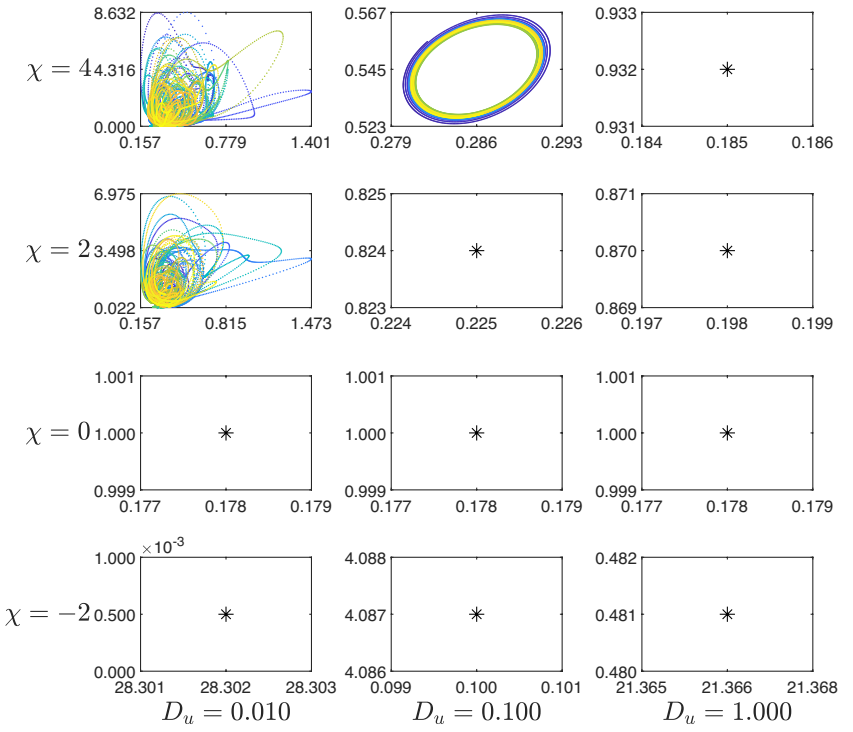


Figure 9. *Solutions to (E) for various D_u (columns) and χ (rows). The non-transient $\rho(\pi/2, t)$ and $u(\pi/2, t)$ are plotted against each other. The remaining parameters are $D_A = 0.1$, $D_\rho = 0.01$, $\alpha = \beta = 1$, $\lambda = (1 + \sqrt{5})/2$. We represent two snapshots using dark blue ($t = 800$) and yellow ($t = 1000$). The star represents the constant-in-time solutions. Here, we note that not only diffusion rates, but other parameters as well, may affect the crime landscape. We observe that the magnitude and sign of χ can significantly impact the local density of both agents, leading to values far from the constant steady state.*

for the parameters given in the caption of Figure 9. In this setting, high police concentration in highly attractive regions prevents the system from reaching spatial uniformity, regardless of adjustments to patrolling (i.e., random movement). In particular, when police movement has no advection component, the system decouples: u converges to a constant steady state, while the remaining scalar fields develop spatially heterogeneous solutions. In this case, the model effectively reduces to a two-component system, which has already been extensively studied in the works referenced in the introduction.

In our simulations, off-hotspot policing is associated with higher crime density and lower police presence, whereas the opposite trend is observed under hotspot policing. For example, in the bottom-left corner of Figure 9, the crime density reaches ≈ 28.3, about 73 times higher than the constant steady-state value. While such disparities may resemble the heterogeneous distribution of crime in urban areas (*cf*, [50]), we emphasize that these findings are model-based and hypothetical. Further empirical validation would be required before drawing any policy implications.

6. Conclusion and brief discussions

We have contributed to the understanding of the pattern formation of a model of urban crime by demonstrating the existence and stability of a nonhomogeneous solution bifurcating from the constant steady state. The bifurcation parameter, χ, does not have any restrictions in terms of its sign and hence a bifurcating point is always defined. The corresponding spatially nonconstant solutions are almost always

https://doi.org/10.1017/S0956792526100357 Published online by Cambridge University Press

present, but they are not always stable. Our approach relies on connecting the central system with the negative Laplacian eigenvalue problem, introduced by Cantrell et al. [8]. This is a powerful tool, as it does not involve the wavemode vector and thus does not explicitly depend on the dimension of the problem. We employed this method to investigate the Hopf bifurcation and obtained a similar result to that derived for the one-dimensional case [39]. One could further extend and show the stability of periodic solutions, but we expect the results to be similar to those in [39]. In addition, we run numerical simulations of system (E), which confirm the theoretical results by demonstrating the existence of orbits. Even when solutions are not periodic, they still may exhibit interesting patterns, whose geometry can be studied as a separate future project. From a theoretical perspective, a worthwhile direction is to analyse chaos, which is only evidenced numerically in this paper, more rigorously. From a practical standpoint, a deeper understanding of various parameter combinations and corresponding solution behaviours needs to be studied as part of a potential comprehensive research design (e.g., how police should move given the current state of the system).

As the work of Cantrell and collaborators [8] complements the work by Short *et al.* [46], this work complements our previous finding in [62], by providing the relevant Theorems. Although the approaches are similar, we note a few differences between this paper and that of Cantrell *et al.* [8]. We have fewer restrictions on the parameter space for the first Theorem, as the control parameter does not have to be positive. On the other hand, we needed to impose more conditions to guarantee stability, as it is "easier" for the relevant characteristic equation to have positive real parts. Cantrell *et al.* stated that the relevant eigenvalues are those that are sufficiently small. This does not appear to be the case for the extended model. We hypothesize that under suitable conditions, any eigenvalue of the negative Laplacian would be relevant. It would be of interest to find the equivalent but simpler assumptions in the theorems. The apparent difference lies in the addition of the third equation, and hence, the increase in dimension from a linear algebra perspective. This comes with challenges, such as dealing with an already non-trivial kernel, third-degree polynomials and more convoluted expressions involving additional parameters, among others. One of the goals of this paper is to demonstrate how to overcome these hindrances, particularly as the number of equations and/or dimensions increases. This is part of a larger effort to investigate pattern formation in the general Keller–Segel model, where analysis has mainly been conducted on systems of two equations. By increasing the model's dimension, one may obtain a more precise picture, but also introduce new complexity. However, with this complexity, new mathematical endeavours and insights emerge, and the authors hope that this paper will serve as a call and a guide to contribute to the field of pattern formation.

Financial support. This work was partially funded by NSF-DMS-2042413 and AFOSR MURI FA9550-22-1-0380.

Competing interests. None.

References

[1] Amann, H. (1991) Hopf bifurcation in quasilinear reaction-diffusion systems. In Busenberg, S. & Martelli, M. (eds.), *Delay Differential Equations and Dynamical Systems*, Springer, Berlin, Heidelberg, Berlin Heidelberg, pp. 53–63.

[2] Barthe, E. P. & Stitt, B. G. (2011) Impact of increased police presence in a non-criminogenic area. *Police Pract. Res.* **12**(5), 383–396.

[3] Berestycki, H. & Nadal, J.-P. (2010) Self-organised critical hot spots of criminal activity. *Eur. J. Appl. Math.* **21**(4-5), 371–399.

[4] Berestycki, H., Wei, J. & Winter, M. (2014) Existence of symmetric and asymmetric spikes for a crime hotspot model. *SIAM J. Math. Anal.* **46**(1), 691–719.

[5] Braga, A. A. (2001) The effects of hot spots policing on crime. *Ann. Am. Acad. Polit. Soc. Sci.* **578**(1), 104–125.

[6] Braga, A. A., Papachristos, A. V. & Hureau, D. M. (2014) The effects of hot spots policing on crime: An updated systematic review and meta-analysis. *Justice Q.* **31**(4), 633–663.

[7] Buttenschoen, A., Kolokolnikov, T., Ward, M. J. & Wei, J. (2020) Cops-on-the-dots: The linear stability of crime hotspots for a 1-D reaction-diffusion model of urban crime. *Eur. J. Appl. Math.* **31**(5), 871–917.

[8] Cantrell, R. S., Cosner, C. & Manásevich, R. (2012) Global bifurcation of solutions for crime modeling equations. *SIAM J. Math. Anal.* **44**(3), 1340–1358.

https://doi.org/10.1017/S0956792526100357 Published online by Cambridge University Press

[9] Chaturapruek, S., Breslau, J., Yazdi, D., Kolokolnikov, T. & McCalla, S. G. (2013) Crime modeling with Lévy flights. *SIAM J. Appl. Math.* **73**(4), 1703–1720.
[10] Crandall, M. G. & Rabinowitz, P. H. (1971) Bifurcation from simple eigenvalues. *J. Funct. Anal.* **8**(2), 321–340.
[11] Crandall, M. G. & Rabinowitz, P. H. (1973) Bifurcation, perturbation of simple eigenvalues and linearized stability. *Arch. Ration. Mech. AnAL.* **52**, 161–180.
[12] D'Orsogna, M. R. & Perc, M. (2015) Statistical physics of crime: A review. *Phys. Life Rev.* **12**, 1–21.
[13] Eck, J. E. (2003). Preventing crime at places. In: Farrington, D. P., MacKenzie, D. L., Sherman, L. & Welsh, B. C. (eds.), *Evidence-Based Crime Prevention*, Routledge, pp. 241–294.
[14] Freitag, M. (2018) Global solutions to a higher-dimensional system related to crime modeling. *Math. Method. Appl. Sci.* **41**(16), 6326–6335.
[15] Frydl, K. & Skogan, W. (2004) *Fairness and Effectiveness in Policing: The Evidence*, National Academies Press.
[16] Gai, C. & Ward, M. J. (2024) The nucleation-annihilation dynamics of hotspot patterns for a reaction-diffusion system of urban crime with police deployment. *SIAM J. Appl. Dyn. Syst.* **23**(3), 2018–2060.
[17] Garcia-Huidobro, M., Manasevich, R. & Mawhin, J. (2013) Existence of solutions for a 1-D boundary value problem coming from a model for burglary. *Nonlinear Anal.: Real World Appl.* **14**(5), 1939–1946.
[18] Groff, E. R., Johnson, S. D. & Thornton, A. (2019) State of the art in agent-based modeling of urban crime: An overview. *J. Quant. Criminol.* **35**, 155–193.
[19] Gu, Yu, Wang, Qi & Yi, G. (2017) Stationary patterns and their selection mechanism of urban crime models with heterogeneous near-repeat victimization effect. *Eur. J. Appl. Math.* **28**(1), 141–178.
[20] Heihoff, F. (2020) Generalized solutions for a system of partial differential equations arising from urban crime modeling with a logistic source term. *Zeitschrift für Angewandte Mathematik Und Physik* **71**(3), 80.
[21] Jiang, W. & Wang, Q. (2024) Global well-posedness and uniform boundedness of 2D urban crime models with nonlinear advection enhancement. *Eur. J. Appl. Math.* **36**(5), 897–909.
[22] Jones, P. A., Brantingham, P. J. & Chayes, L. R. (2010) Statistical models of criminal behavior: The effects of law enforcement actions. *Math. Models Methods Appl. Sci.* **20**(supp01), 1397–1423.
[23] Kleck, G. & Barnes, J. C. (2014) Do more police lead to more crime deterrence? *Crime Delinq.* **60**(5), 716–738.
[24] Kolokolnikov, T., Ward, M. J. & Wei, J. (2014) The stability of steady-state hot-spot patterns for a reaction-diffusion model of urban crime. *Discrete Contin. Dyn. Syst.-B* **19**(5), 1373–1410.
[25] Kumar, M. & Abbas, S. (2023) Modelling and prevention of crime using age-structure and law enforcement. *J. Math. Anal. Appl.* **519**(2), 126849.
[26] Ladyzhenskaia, O. A. & Ural'tseva, N. N. (1968) *Linear and Quasilinear Elliptic Equations*, Vol. 46 of Mathematics in Science and Engineering. Academic Press.
[27] Levajković, T., Mena, H. & Zarfl, M. (2016) Lévy processes, subordinators and crime modelling. *Novi Sad J. Math.* **46**(2), 65–86.
[28] Lloyd, D. J. B. & O'Farrell, H. (2013) On localized hotspots of an urban crime model. *Physica D: Nonlinear Phenom.* **253**, 23–39.
[29] Lloyd, D. J. B., Santitissadeekorn, N. & Short, M. B. (2016) Exploring data assimilation and forecasting issues for an urban crime model. *Eur. J. Appl. Math.* **27**(3), 451–478.
[30] Manasevich, R., Phan, Q. H. & Souplet, P. (2013) Global existence of solutions for a chemotaxis-type system arising in crime modeling. *Eur. J. Appl. Math.* **24**(2), 273–296.
[31] Martínez-Farías, F. J., Alvarado-Sánchez, A., Rangel-Cortes, E. & Hernández-Hernández, A. (2022) Bi-dimensional crime model based on anomalous diffusion with law enforcement effect. *Math. Model. Numer. Simul. Appl.* **2**(1), 26–40.
[32] Mei, L. & Wei, J. (2020) The existence and stability of spike solutions for a chemotaxis system modeling crime pattern formation. *Math. Models Methods Appl. Sci.* **30**(09), 1727–1764.
[33] Mohler, G. O. & Short, M. B. (2012) Geographic profiling from kinetic models of criminal behavior. *SIAM J. Appl. Math.* **72**(1), 163–180.
[34] Mohler, G. O., Short, M. B., Brantingham, P. J., Schoenberg, F. P. & Tita, G. E. (2011) Self-exciting point process modeling of crime. *J. Am. Stat. Assoc.* **106**(493), 100–108.
[35] Pan, C., Li, B., Wang, C., et al. (2018) Crime modeling with truncated Lévy flights for residential burglary models. *Math. Models Methods Appl. Sci.* **28**(09), 1857–1880.
[36] Pitcher, A. B. (2010) Adding police to a mathematical model of burglary. *Eur. J. Appl. Math.* **21**(4-5), 401–419.
[37] Ricketson, L. (2010) A continuum model of residential burglary incorporating law enforcement. preprint on webpage at www.academia.edu/570840/A_Continuum_Model_of_Residential_Burglary_Incorporating_Law_Enforcement
[38] Rodríguez, N. (2013) On the global well-posedness theory for a class of PDE models for criminal activity. *Physica D: Nonlinear Phenom.* **260**, 191–200.
[39] Rodríguez, N., Wang, Q. & Zhang, L. (2021) Understanding the effects of on-and off-hotspot policing: Evidence of hotspot, oscillating, and chaotic activities. *SIAM J. Appl. Dyn. Syst.* **20**(4), 1882–1916.
[40] Rodríguez, N. & Winkler, M. (2022) On the global existence and qualitative behavior of one-dimensional solutions to a model for urban crime. *Eur. J. Appl. Math.* **33**(5), 919–959.
[41] Rosenbaum, D. P. (2006). The limits of hot spots policing. In: Weisburd, D. & Braga, A. A. (eds.), *Police Innovation: Contrasting Perspectives*, Cambridge University Press, pp. 245–263.
[42] Saldana, J., Aguareles, M., Avinyó, A., Pellicer, M. & Ripoll, J. (2018) An age-structured population approach for the mathematical modeling of urban burglaries. *SIAM J. Appl. Dyn. Syst.* **17**(4), 2733–2760.

https://doi.org/10.1017/S0956792526100357 Published online by Cambridge University Press

[43] Sampson, R. J. & Raudenbush, S. W. (2004) Seeing Disorder: Neighborhood stigma and the social construction of "Broken Windows". *Soc. Psychol. Quart.* **67**(4), 319–342.
[44] Sherman, L. W. & Weisburd, D. (1995) General deterrent effects of police patrol in crime "hot spots": A randomized, controlled trial. *Justice Q.* **12**(4), 625–648.
[45] Shi, J. & Wang, X. (2009) On global bifurcation for quasilinear elliptic systems on bounded domains. *J. Differ. Equations* **246**(7), 2788–2812.
[46] Short, M. B., Bertozzi, A. L. & Brantingham, P. J. (2010) Nonlinear patterns in urban crime: Hotspots, bifurcations, and suppression. *SIAM J. Appl. Dyn. Syst.* **9**(2), 462–483.
[47] Short, M. B., Brantingham, P. J., Bertozzi, A. L. & Tita, G. E. (2010) Dissipation and displacement of hotspots in reaction-diffusion models of crime. *Proc. Natl. Acad. Sci.* **107**(9), 3961–3965.
[48] Short, M. B., D'orsogna, M. R., Pasour, V. B., et al. (2008) A statistical model of criminal behavior. *Math. Models Methods Appl. Sci.* **18**(supp01), 1249–1267.
[49] Skogan, W. G. & Hartnett, S. M. (1999) *Community Policing, Chicago Style*, Oxford University Press.
[50] Thacher, D. (2011) The distribution of police protection. *J. Quant. Criminol.* **27**, 275–298.
[51] The MathWorks Inc. (2024) MATLAB Version R2024b. Natick, MA.
[52] The MathWorks Inc. (2024) Partial Differential Equation Toolbox, Version R2024b. Natick, MA.
[53] Tse, W.-H. & Ward, M. J. (2016) Hotspot formation and dynamics for a continuum model of urban crime. *Eur. J. Appl. Math.* **27**(3), 583–624.
[54] Tse, W.-H. & Ward, M. J. (2018) Asynchronous instabilities of crime hotspots for a 1-D reaction-diffusion model of urban crime with focused police patrol. *SIAM J. Appl. Dyn. Syst.* **17**(3), 2018–2075.
[55] Wang, Qi, Wang, D. & Feng, Y. (2020) Global well-posedness and uniform boundedness of urban crime models: One-dimensional case. *J. Differ. Equations* **269**(7), 6216–6235.
[56] Wang, Qi, Yang, J. & Zhang, L. (2017) Time-periodic and stable patterns of a two-competing-species Keller-Segel chemotaxis model: Effect of cellular growth. *Discrete Contin. Dyn. Syst.-B* **22**(9), 3547–3574.
[57] Weisburd, D. & Eck, J. E. (2004) What can police do to reduce crime, disorder, and fear? *Ann. Am. Acad. Pol. Soc. Sci.* **593**(1), 42–65.
[58] Weisburd, D. & Green, L. (1995) Policing drug hot spots: The Jersey City drug market analysis experiment. *Justice Q.* **12**(4), 711–735.
[59] Weisburd, D., Telep, C. W., Hinkle, J. C. & Eck, J. E. (2010) Is problem-oriented policing effective in reducing crime and disorder? Findings from a campbell systematic review. *Criminol. Public Pol.* **9**(1), 139–172.
[60] Wilson, J. Q. & Kelling, G. L. (1982) Broken windows: The police and neighborhood safety. *Atlantic Monthly* **249**(3), 29–38.
[61] Winkler, M. (2019) Global solvability and stabilization in a two-dimensional cross-diffusion system modeling urban crime propagation. *Annales De l'Institut Henri Poincaré C, Analyse Non Linéaire* **36**(6), 1747–1790.
[62] Yerlanov, M., Wang, Q. & Rodríguez, N. (2025) Formation and suppression of hotspots in urban crime models with law enforcement. *Chaos: An Interdisciplinary Journal of Nonlinear Science* **35**(6), 1–17.
[63] Zipkin, J. R., Short, M. B. & Bertozzi, A. L. (2014) Cops on the dots in a mathematical model of urban crime and police response. *Discrete Contin. Dyn. Syst.-B* **19**(5), 1479–1506.

Cite this article: Yerlanov M., Wang Q. and Rodríguez N. (2026). Global bifurcations and pattern formation in target–offender–guardian crime models. *European Journal of Applied Mathematics*, **37**, 1313–1341. https://doi.org/10.1017/S0956792526100357

https://doi.org/10.1017/S0956792526100357 Published online by Cambridge University Press